UNIVERSITY OF NICOSIA

CONSTRUCTION OF A VARIABLE INTEGRATED INDUCTOR-CAPACITOR FOR REACTIVE POWER COMPENSATION

VIJAYA KRISHNA SATYAMSETTI

PhD (Doctor of Philosophy)

in

ELECTRICAL ENGINEERING

MAY 2022

UNIVERSITY OF NICOSIA

CONSTRUCTION OF A VARIABLE INTEGRATED INDUCTOR-CAPACITOR FOR REACTIVE POWER COMPENSATION

VIJAYA KRISHNA SATYAMSETTI

A thesis submitted to the University of Nicosia

in accordance with the requirements of the degree of

PhD (Doctor of Philosophy) in Electrical Engineering

Department of Engineering

School of Sciences and Engineering

May 2022

Abstract

This thesis presents an integrated inductor-capacitor wound from aluminum/polyester foils and examines its suitability to provide variable reactive power for compensation in low voltage power systems. Explaining the functional concept of this integrated component shows how its terminal impedance can be adjusted to be either capacitive or inductive. A 15 kVAR prototype integrated component is wound. Measured technical parameters of the pilot model like capacitance, inductance and resistance match satisfactorily respective values in the calculation scheme of the preceding components' design, thus verifying its dual character.

The next stage enabling qualified analysis of this component is the derivation of its equivalent circuit. The integrated inductor-capacitor wound from aluminum and polyester foils measures constant parameters and hence provides the possibility for limited experimentation. Employing, however, the equivalent circuit, instead of the integrated inductor-capacitor, displaying the same operational behavior but constructed from discrete components as resistors, inductors and capacitors widely available in the market in big variety and easily exchangeable in the circuit provides multiple and diverse experimental possibilities. This may avoid winding components of various parameters with materials of different sizes requiring particular winding equipment, thus exceeding the current scope of experimentation. Finally, the significance of presenting the integrated inductor-capacitor via an equivalent is the possibility to express its terminal impedance as a function of its technical parameters, R, L and C.

The realized equivalent circuit, constructed from discrete components can provide throughout a considerable range of capacitive up to inductive reactive power. In the experimental part to follow, a specially constructed circuit

replicating the equivalent circuit is regulated by a variable resistor at the load terminals 2-4 in order to provide the exact capacitive reactive power required to compensate the phase shift in the system caused by a single phase induction motor. The same circuit provides, during further experimentation via regulation of the variable resistor, inductive reactive power thus compensating the leading phase shift of the simulated capacitive load. Adjusting the circuit's terminal impedance is being achieved via a variable resistor. Considerable losses, converted in the equivalent circuit when regulated with variable resistor in order to provide the required reactive power, are of major concern. Because of this the possibility is being examined to regulate the equivalent circuit's impedance with an air wound inductor. This variable inductor functions on the principle of mutual inductance.

In further measurements documenting the ability of the actual foil wound component to perform automatic compensation, the reactive power of a 1.2 kW, 230 V induction motor is compensated by the initial constructed pilot model, the latter being regulated to provide the necessary capacitive reactive power via the variable inductor. Continuous monitoring of the system constituted by the induction motor and the integrated component assess the phase and consequently regulates automatically the component's terminal impedance thus maintaining unity power factor in the system, despite varying load. Extended experimentation indicates reasonable prospects for the integrated component to provide VAR compensation.

Keywords: Foil wound capacitors and inductors, integrated capacitor inductor, power factor correction, power quality and reactive power compensation.

"Respects to Mother, Father and Guru. They are all forms of Gods"...

Taittiriya Upanishad

Acknowledgements

Thinking back on the last 5 years of my life in Cyprus, I can't imagine having a better time and experience. Just a week away from graduation, and it's surreal to know that I am almost at the finish line. I would be very remiss of me if I did not take time to acknowledge the people that have helped and encouraged me along the way.

First, and foremost, I would like to express my extreme gratitude to my advisor, Dr. Andreas Michaelides, for always being both present, calm, kind and patient force during my journey. He taught me countless invaluable lessons in research and academics. Many times, I would go into our weekly one-on-one meetings ready to implode. Every word in a conservation with him is a life-long advice. His level of optimism always amazed me, and proved to me that nothing is impossible! Dr. Michaelides was always more than just an academic advisor to me, more like a god father in my life and I want to thank him for always having faith in me and letting me load any type of work.

In addition to Dr. Michaelides, I would like to thanks my co-advisor, Dr. Antonis Hadjiantonis for years of guidance and mentorship maintaining an exciting research environment within the group. Further, I would like to show my extreme gratitude to another co-advisor Dr. Stelios Hirodontis, for always being kind and supporting me during this journey.

A sincere thanks goes out to the Engineering Department faculty members particularly, Andreas Sergiou and Stelios Neophytou for their invaluable help. To my family I owe everything. I thank my mother who provided me with the inspiration to go abroad for pursuing a PhD. And I thank my father and sister for their unwavering support and endless encouragement through my life. I owe a special thanks to my brother, who was a great inspiration in my life and a main reason for me to continue my graduate studies.

Declaration

I declare that the work in this thesis was carried out in accordance with the regulations of the University of Nicosia. This thesis has been composed solely by myself except where stated otherwise by reference or acknowledgment.

It has not been previously submitted, in whole or in part, to this or any other institution for a degree, diploma or other qualifications.

Signed …....…….. Date ……...……

Name Surname

Contents

List of Figures

List of Tables

List of Abbreviations

AC	**A**leternating **C**urrent
CMOS	**C**omplementary **M**etal **O**xide **S**emiconductor
CSI	**C**urrent **S**ource **I**nverter
DC	**D**irect **C**urrent
FACTS	**F**lexible **A**lternating **C**urrent **T**ransmission **S**ystems
LV	**L**ow **V**oltage
PF	**P**ower **F**actor
PV	**P**hoto **V**oltaic
PQ	**P**ower **Q**uality
PFCU	**P**ower **F**actor **C**orrection **U**int
RF	**R**adio **F**requency
RES	**R**enewable **E**nergy **S**ources
SVC	**S**tatic **V**AR **C**ompensator
STATCOM	**S**tatic **S**ynchronous **C**ompensator
TSC	**T**hyristor **S**witched **C**apacitor
TCR	**T**hyristor **C**ontrolled **R**eactor
THD	**T**otal **H**armonic **D**istrotion
VAR	**V**olt **A**mpere **R**eactive
VSI	**V**oltage **S**ource **I**nverter

List of Symbols

C	Capacitance	μF
D_i	Integrated component core diameter	cm
D_o	Integrated component outer diameter	cm
h	Nagaoka coefficient	
I	Current	A
k	Coupling factor	
l_{Al}	Total length of foils	m
L	Inductor	mH
l	Length of aluminum	m
l_{seg}	Length of segment	m
n	Number of segments	
N	Number of soil turns	
P	Power	W (J s^{-1})
Q_C	Capacitive reactive power	VAR
Q_L	Inductive reactive power	VAR
Q	Quality factor	
R	Resistance	Ω
S_{Al}	Aluminum foils strength	μm
S_{pp}	Polyester foils strength	μm
V	Voltage	V
w_{Al}	Aluminum foils width	cm
ε_r	Polyester foils dielectric	
ρ_{Al}	Aluminum resistivity	Ωm
μ_o	Permeability of free space	Vs/Am
ω	Angular Frequency	rad

Chapter 1

Introduction

This chapter gives a brief background on reactive power compensation techniques and explains why VAR compensation is an appropriate solution for power system quality. The scope of the thesis is then introduced and the scientific objectives of the work are described. The chapter presents the innovation and originality of the work, lists the scientific papers included in the thesis, and provides an outline of the work/terminology.

1.1 Importance of the Work

Today's power transmission and distribution networks continuously expand to cover new residential and/or industrial developments. In addition, there is a parallel, rapidly growing need for evolution as Renewable Energy Sources penetrate deeper into the existing infrastructures requiring fast responses to ever-changing conditions (Jaramillo, Heydt, and O'Neill-Carrillo, 2000), (Lin and Domijan, 2005). Concurrently, as electricity is already a necessity in today's socioeconomic fabric, it is paramount that the grid also provides reliable, cheap and high-quality power without burdening its elements with additional electrical or thermal stress. This extra stress comes typically in the form of reactive currents that are not contributing to any actual work and it is thus desirable to minimize them.

The above create the need for a dynamic grid behavior. Grids nowadays are expected to sense and dynamically react to network changes in order to avoid potential temporary breakdowns or even complete blackouts. In addition, a manifestation of good power quality has traditionally been minimum voltage level fluctuations. These fluctuations are traditionally caused by the lines' resistances and loads and quite predictable in nature (one needs to consider the grid topology, the line length and expected loads to understand the problem). To mitigate this on the low voltage (LV) grid owners make use of

transformer tapping (Tap changing transformer) to control the starting voltage level and ensure that all the voltage experienced by the users is around the nominal value.

With the advent of renewable energy sources(RES) and decentralized production, power is produced and injected to the grid at various locations. To realize these injections, the RES slightly raise the voltage at the production sites. As RES distributed production of small, yet many, residential Photovoltaic (PV) systems on the LV grid becomes important, the above situation becomes severe and the consequent problem more complex and more difficult to predict and rectify. Consequently, static or stepped approaches are rendered ineffective.

The objective of this work is to design, minimize, construct and experimentally investigate a fully-functional, elastic, power factor improvement device that will enhance voltage regulation and reduce reactive power to the LV grid. The device will be capable of sensing current distribution grid conditions and automatically respond by providing the exact reactive component required for stabilization and improvement.

1.2 Background

Industrial plants (mainly factories) cause, through their predominantly motor loads, lagging power factor to the grid. Domestic and urban loads in general, likewise, cause lagging power factor, though to a lesser extent. On the other hand, increased employment of underground middle range voltage cables (eg: 11 kV) over distances of tens of kilometers and more cause a definite leading power factor due to the high parasitic capacitance arising between the closely positioned phase conductors of the cables. Both lagging and leading power factors cause additional voltage drop/rise, losses on the transmission lines and in general a power quality deterioration, forcing the providers to undertake qualified actions aiming at countering negative effects resulting from the phase shift. Overall, reactive power management is classified into two categories (a) transmission-line voltage (b) load delivered (T.J.Miller, 2017), (Dixon et al., 2005). Voltage control typically refers to eliminating the voltage fluctuations, improving the stability of voltage and maintaining a flat voltage profile at various levels of transmission. The second category is load delivered, which has to do with the enhancement of the power factor, the consumption of real power from the supply, voltage regulation and the reduction of the total harmonic distortion (THD) caused

by large nonlinear loads (Teleke et al., 2008). The issues appearing because of the inability to control the reactive power are significant. Untill recently, the active and reactive power was controlled by conventional techniques like automatic generation control (AGC), excitation control, phase-shifting transformers, transformer tap-changing control, capacitor systems (capacitor banks, parallel capacitors), and Thyristor based controllers (T.J.Miller, 2017), (R.Mohan Mathur, 2002). In general, there are two basic approaches for compensating the phase shift (i.e correcting the power factor): static and dynamic.

1.2.1 Static Compensation

The simplified equivalent circuit (given in Figure 1.1) of a motor load is a resistor representing the converted mechanical power, and a parallel inductor necessary to set up the magnetic field in the windings and create the mechanical force. This arrangement causes a lagging power factor, that is, the current lags the voltage by some time.

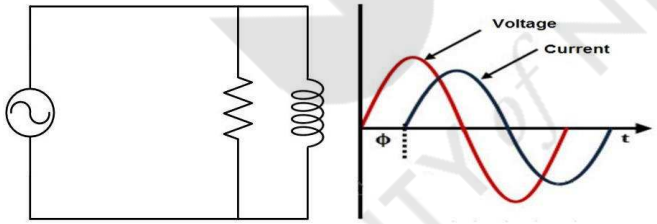

FIGURE 1.1: Equivalent of motor load

Hence, capacitor banks (Figure 1.2) are being installed in the factory premises to provide capacitive reactive power in order to completely mitigate or eliminate this lagging power factor on the spot. Now, as the production process in factories varies, that is motors of different power ratings are constantly connected and disconnected many times without a predetermined pattern, a central power factor correction unit (PFCU) keeps connecting and disconnecting components from a local capacitor bank automatically, via electromechanical switches (Fehr, 2016) as shown in Figure 1.3.

These reactive components are usually power capacitors of different sizes designed appropriately to regulate the power factor of a specific plant (whose overall reactive compensation needs are expected) to a desired value. At any moment, the connected capacitance (i.e. engaged reactive components) is

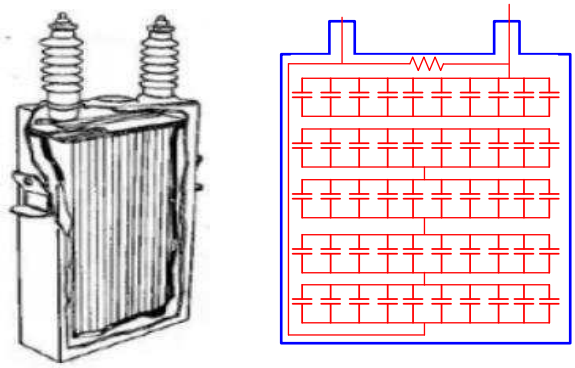

FIGURE 1.2: Capacitor bank and its equivalent

FIGURE 1.3: Mechanically switched capacitors
(Source: Siemens Energy)

the sum of the various discrete capacitor components used. As there are no variable power capacitors, a constant switching of capacitors is normally realized, especially for those of lower capacitances. The problem arising when this kind of switching is employed has to do with the large inrush current that flows at the moment of contact when the instantaneous voltage difference between the line and the capacitor is big. This is shown in Figure 1.4.

This high inrush current reduces considerably the capacitor's overall operational duration which, frequently, ends in mini-explosions. In some cases power authorities install capacitor banks in substations for central compensation, especially when individual customers (usually home or small commercial units) exhibit insignificant phase shifts but as a group cause significant effects.

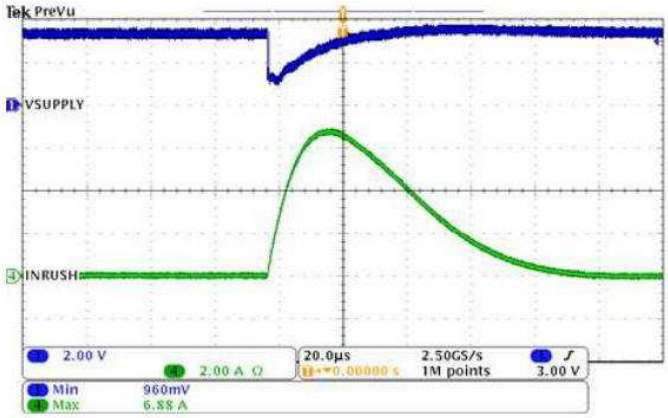

FIGURE 1.4: Voltage sag due to inrush current
(Source:Texas Instruments Manual-Inrush Currents)

Leading power factors caused by underground cables that run close to power stations can be compensated by under-exiting the synchronous generator. This means that the generator provides real power and, at the same time, absorbs reactive power. In addition, when reactive power compensation in substations is needed, the so called synchronous compensators are often installed (Ma et al., 2016), shown in Figure 1.5.

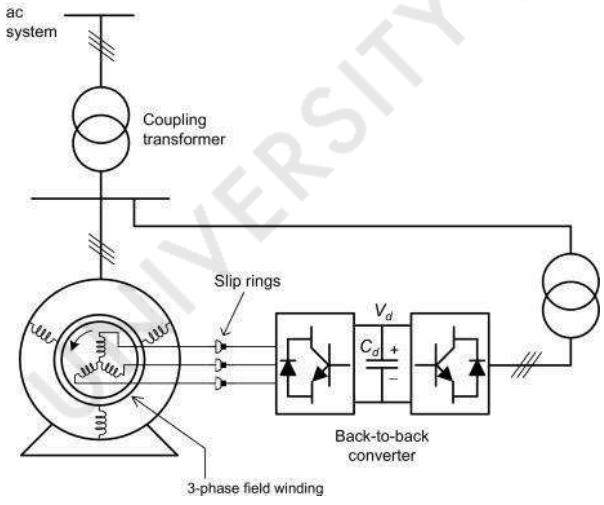

FIGURE 1.5: Synchronous condenser with variable speed

These generators are synchronous machines made to rotate at synchronous speed with no mechanical torque given to the shaft; the active power delivered by the network corresponds to the power loss of the machine. With

excitation, the operating point typically moves on the axis of the reactive power and the machine behaves as either a condenser or an inductance. Synchronous condensers used to compensate phase shifts caused by underground cables leaving the substations. However, for this type of compensator to be used at full efficiency, it should be driven in a closed chamber full of hydrogen so as to reduce the losses by ventilation and to increase the specific power. The cost of such system is high and encumbering. For this reason, capacitive power compensation is being achieved in many European countries by installing bulky air-cooled inductors. The value of inductors can be changed by choosing suitable taps. In big inductors the length/depth of immersing an iron core via an electric motor changes the inductance gradually.

1.2.2 Dynamic Compensation

With the advance of thyristors in the early 80s, typical AC bidirectional switches were developed for controlling (connecting and disconnecting) the capacitor banks (Jovanovic and Jang, 2005)(Sebastian and Jaureguizar, 1993)(Chavez and Houdek, 2007) (Pop et al., 2001). A bank of capacitors connected using anti parallel thyristor pairs as per Figure 1.6 is commonly known as Thyristor-Switched Capacitor (TSC) .

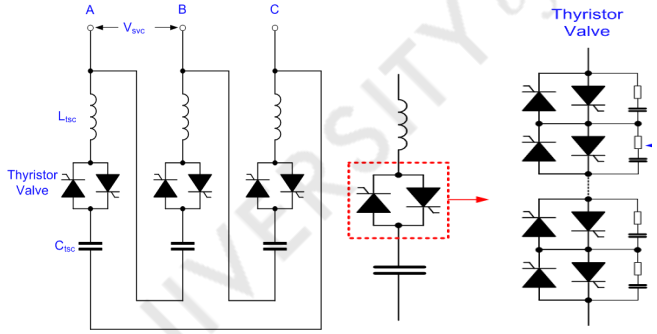

FIGURE 1.6: TSC used for mitigation of the capacitor inrush currents

TSCs overcome the inrush current problem because they use thyristor valves which can be triggered at any point of the AC waveform by means of processor controllers that constantly sense the voltage difference. If TSCs alone are employed for reactive power compensation, the introduced leading VAR can only be adjusted in steps, because the switching is realized one reactive component at a time. For accurate adjustments of VAR, a continous

variable feature is desirable. This is achieved by having a thyristor-controlled reactor (TCR) (Rahmani et al., 2014)(Chen, Lee, and Chen, 1999)(Haque, Malik, and Shepherd, 1985), as shown in Figure 1.7, in parallel with the capacitor bank (detuned reactor) as shown in Figure 1.8 called static-VAR compensators (SVC) .

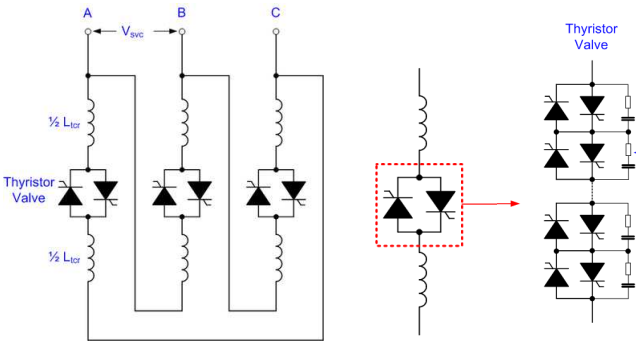

FIGURE 1.7: Thyristor-controlled reactor

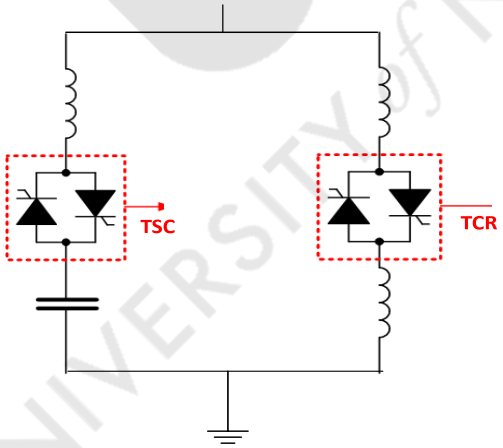

FIGURE 1.8: TCR in parallel with capacitor bank (SVC)

In general, these compensators are more reliable, faster and have a higher capacity compared to synchronous condensers. However, SVCs are of comparably higher cost than conventional (mechanically switched) capacitor banks, due to complex processor controlled electronics involvement, need new technologies and require quick support. At present, power electronic controllers such as voltage source inverters (VSI)/ current source inverters (CSI) based static-VAR compensators (SVC and STATCOM) (Dixon et al., 2005),(Narain

G. Hingorani, 1999),(R.Mohan Mathur, 2002), (Yong Hua Song, 2008) are widely used for VAR compensation often called flexible aternating current transmission systems (FACTS), shown in Figure 1.9.

FIGURE 1.9: Typical SVC (source: GE grid solutions)

Although power electronics can achieve accurate and dynamic power factor control, the latter suffers from frequent thyristor failures caused by switching and, thus, the consequent nesessity for justifying the continued use of static compensation.

1.3 Scope of the Work

The final device that the current work intends to build is an apparatus within the technical area of electric power quality. The electric device shall be capable to either inject or absorb reactive power to/from the grid accounting for load units that cause phase shift, hence reduce the power factor, both towards the lagging as well as the leading regime. It is the device's constructional nature that yields, in one component, capacitance and inductance. It is further the specific design and operation that can drive this electric device from a capacitive extreme all the way through to an inductive extreme by both manually controlled resistor and variable inductor employing microprocessor control. However, the most significant feature of this device is the possibility to realize different capacitive and inductive values as well as to change its electrical behavior from capacitive to inductive without switching between the device and the grid to which it is already connected. Hence the

considerable advantage of the proposed apparatus to any existing device system performing the same function, apart from its accurate compensation, is its expected long operational duration. The constantly monitored grid shall provide information about its current state to the control system of the device which, in turn, will respond with steady adjustment to appropriate dynamic changes of particular load scenarios in the grid taking on the new operating mode so as to realize the predetermined desired grid parameters. Current construction concept aims at a LV, 400V, 3-phase device.

The electrical device that this thesis will produce will be capable to provide the following:

- One device will be capable to correct both leading and lagging power factors;
- It will be capable to compensate reactive components elastically (not in steps);
- It will exhibit prolonged useful life as it will not employ capacitor switching;
- It will not generate harmonics like TCR and will need no additional filtering;
- It will respond to unfavorable changes in the grid in real-time.

To the best of my knowledge, at present, there is no available, marketable device to manage reactive power cost-effectively in the above manner.

1.4 Thesis Objectives

The aim of this thesis is to construct an integrated component providing both inductive and capacitive reactive powers for medium and high power applications as a VAR compensator. The scientific and technical objectives of the thesis are:

- Create a device whose constructional nature allows it to both inject and absorb reactive power to and from the LV grid ;
- Replace the conventional engagement/disengagement of discrete power components with a smooth and gradual, (“elastic”), compensation;

- Achieve the above without the use of power electronics (thyristors) which deteriorate the power quality and introduce the need for filtering.

The first objective is to construct an electric device that will inject or absorb reactive power to and from the grid accounting for motor load (and/or parasitic capacitances in underground cable runs) that causes phase shift and reduces the power factor (PF) both towards lagging as well as leading regions. This implies that a single device will be capable of delivering capacitive as well as inductive reactive power. The basic principle of the design of such a device is the integrated reactive component that has been theoretically known in the literature and has been used in various applications (eg: in the starting and operation of induction motors (Michaelides and Nicolaou, 2017b) and in harmonic filtering techniques (Michaelides, 2015) etc). When studied, its electrical characteristics reveal that with the appropriate circuit around, it can behave between the two extremes; a series and a parallel resonance.

In addition, the device will be able to vary the amount of reactive power it compensates elastically, changing gradually and smoothly from a maximum capacitive reactive to a maximum inductive reactive behavior. This avoids the employment of discrete reactive power components to achieve the compensation. Moreover, it avoids the life-shortening switching process used in traditional Power Factor Correction Units (PFCU) where discrete capacitors in a capacitor bank are abruptly engaged or disengaged to reach the required amount of reactive power to be injected to the system. Importantly, this elastic compensation and flexibility in absorbing or injecting reactive power will not be achieved with the use of thyristor-based power electronics.

Another significant objective of this work is to allow the device to realize the above changes of the electrical behavior (from capacitive to inductive), thus enabling it to respond and adjust to appropriate dynamic changes of particular loads in the grid, automatically and in real time. The constantly monitored grid shall provide information about its current state to the control system of the device which, in turn, using a microprocessor will take on the new operating mode so as to realize the predetermined desired grid parameters. Current construction concept aims at the LV (four hundred volts), three phase and around 15 kVAR device. Thanks to the speed, with which the device can respond to unfavorable changes in the grid, it will be amending them immediately, if necessary. This is in contrast to the currently used

devices that require time delays to switch components (e.g. 30 seconds to engage and up to a minute to disengage) in order to avoid the harmful frequent switching processes.

Currently, a device capable to perform the above tasks in the explained manner does not exist in the market. While the theory and mathematics behind the approach all seem to indicate that the device can be constructed, this thesis will attempt to actually construct it in order to reveal and overcome any unforeseen technological or scientific hurdles in the process.

1.5 Innovation and Originality

The basic structure of the proposed device is a reel of wound conducting and insulating foils encoutered in conventional discrete foil-wound capacitors, but with novel features in the division of the foils, the sequence of their winding and interconnection with sole objective the maximum exploitation of the inductance following the concept of foil-wound inductors.

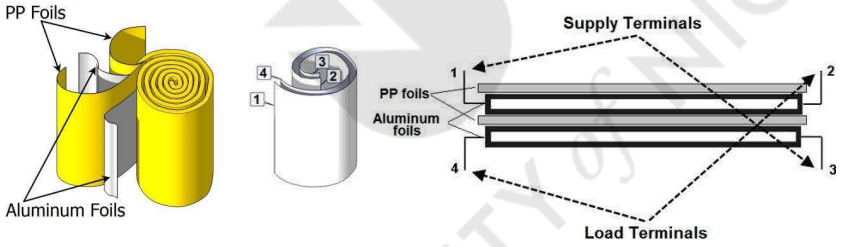

FIGURE 1.10: Conventional capacitor construction and four terminal concept

The apparatus is constructed using two conducting (aluminum) foils isolated by insulating (e.g. polyester) foils as being practiced in the construction of conventional wound film capacitors as shown in Figure 1.10(left). The two opposite ends of the two different foils show the supply terminals (1 and 3) of the proposed integrated inductor-capacitor, and the other two terminals (2 and 4) of the two ends act as control terminals/load terminals as shown in Figure 1.10(right).

Operating the device with high load resistance (e.g. 200 KΩ terminals 2 and 4 shown in Figure 1.11) will yield an impedance frequency characteristic that passes through point P2 at 50 Hz shown in Figure 1.12. Similarly, shorting the same load terminals will result to a function passing through point P1 at 50Hz. Continuing to perform measurements, we can determine the

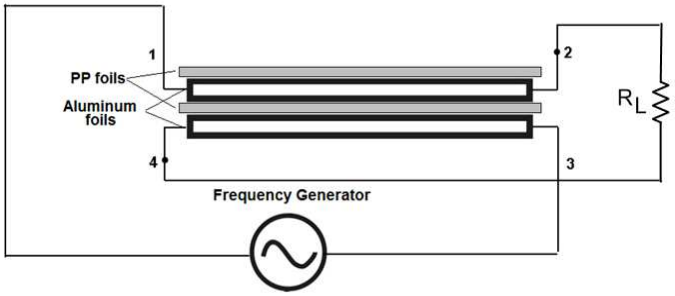

FIGURE 1.11: Impedance at supply (terminals 1 and 3) changes when changing load resistance (terminals 2 and 4)

impedance-frequency characteristic for various resistance values in between the above extremes, which will yield the spectrum lines of Figure 1.12. What is most important is that we can achieve a gradual and smooth transition from the one curve to the other by gradually varying the resistance.

Observing Figure 1.12 further, it is understood that the terminal impedance of the proposed component operating at 50 Hz line frequency changes gradually from one state (inductive) at P1, to another state(capacitive) at P2 along the dotted vertical line. An automatic terminal impedance control of the proposed component can be achieved by controlling the current in the load loop which has initially been managed by a variable resistor with a cost of active power loss. To overcome this loss, a high efficient variable inductor has been examined employing a stepper motor control to perform automatic VAR compensation (introduced in Chapter 4).

To achieve an immediate response of the device to grid changes a processor control unit will collect the phase and process continuously. According to a desired value (grid phase angle), the processor will adjust the current in the load loop so that the device will output the required impedance which will translate to the exact required component to compensate for the excess grid reactive power.

So, by controlling the basic integrated design at this point via a variable impedance, it will be demonstrated that the structure can behave between two extremes: a series and a parallel resonance circuit (points P2 and P1 in Figure 1.12) and that the transition from one to the other will be elastically achieved (i.e. without steps or switching). The two resonances will eventually lead to injecting and absorbing reactive power to/from the grid.

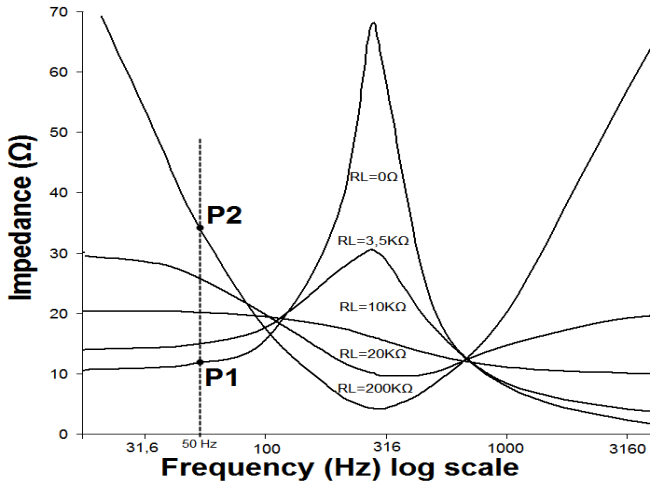

FIGURE 1.12: Impedance frequency characteristics for different control/load resistances showing their locus at line frequency 50Hz

1.6 Discussion

The true technical innovation and originality of the device is to use wound foils as an integrated inductive-capacitive component in transmission system as shown in Figure 1.13:

- For electric power processing application to control the phase between current and voltage in the power system.
- For varying its terminal impedance through an angle of at least 140 degrees meaning that it can shift between capacitive and inductive behavior without any switching.

Since no complex power electronics will be involved (as with dynamic compensations) and there will be monitoring of its performance and status, we expect the device to be low-maintenance and cost-effective. In addition, it will be less bulky than deploying similarly sized solutions (static compensators) while performing the task of both inductors and capacitors. These, along with the elastic compensation it will be capable of, will render such a device easy to market and promote to the local and international industrial markets. Such a device will mitigate the problems arising from sudden, modern grid changes, be they due to complex, ever-extending infrastructure, due to industrial applications, or due to RES decentralized production, thus allowing resilient and quality power delivery.

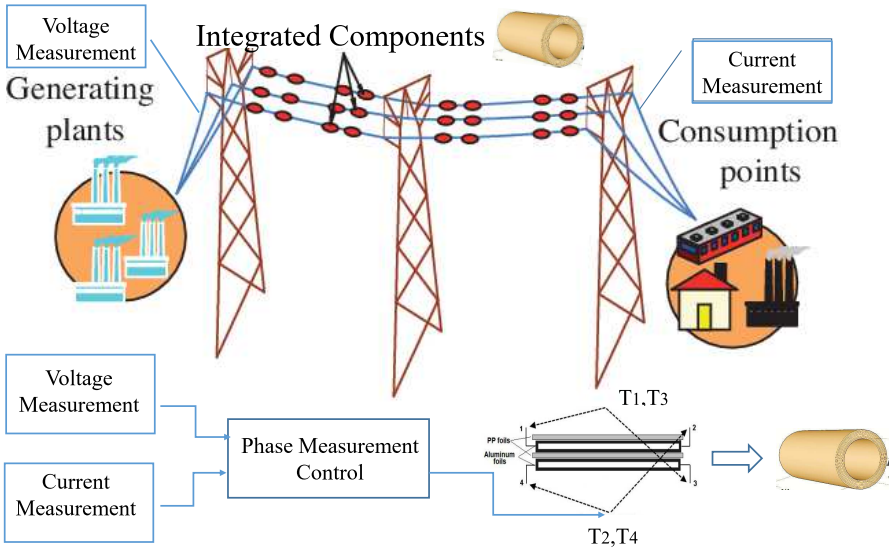

FIGURE 1.13: Main components of the proposed final device

1.7 Publications

- **V. Satyamsetti**, A. Michaelides, A. Hadjiantonis and T. Nicolaou, "A Novel Simple Inductor-Controlled VAR Compensator," in IEEE Transactions on Circuits and Systems II: Express Briefs, vol. 69, no. 2, pp. 524-528, Feb. 2022, doi: 10.1109/TCSII.2021.3099876.

- **V. Satyamsetti**, A. Michaelides, A. Hadjiantonis and T. Nicolaou, "Construction of a Variable Integrated Inductor-Capacitor for VAR Applications," in IEEE Transactions on Power Delivery, (Under review).

- A. Michaelides, T. Nicolaou, D. Afxentiou and **V. Satyamsetti**, "An Adjustable Integrated Inductive Capacitive Component to Compensate Reactive Power," IEEE 2019 15th International Conference on Engineering of Modern Electric Systems (EMES), 2019, pp. 65-68.

- **Satyamsetti, V. K.**; Michaelides, A.; Hadjiantonis, A.: 'ACTIVE COMPENSATION OF REACTIVE POWER VIA STATCOM ANALYSIS', IET Conference Proceedings, 2021, p. 121-126, DOI: 10.1049/icp.2021.1252, IET Digital Library, https://digital-library.

- **V. Satyamsetti**, A. Michaelides, A. Hadjiantonis, A. C. Polycarpou and T. Nicolaou, "Small-Size, Low-Weight, Single-Phase Inverter for Domestic Applications," IEEE 2018 53rd International Universities Power Engineering Conference (UPEC), 2018, pp. 1-6.

- **V. Satyamsetti**, A. Michaelides, A. Hadjiantonis and A. C. Polycarpou, "Design and Analysis of a High-Frequency 3-Phase Distributed Static Compensator (HFDSC)," IECON 2018 - 44th Annual Conference of the IEEE Industrial Electronics Society, 2018, pp. 3609-3614, doi: 10.1109/IECON.2018.8591370.

1.8 Organization of Thesis

This thesis is structured as follows:

- **Chapter 1** offers an explanation for the general reader about the reactive power compensation. The motivation for the research, the aim and thesis outline, and the main scientific contributions are also included in this chapter.
- **Chapter 2** presents the concept of integrated inductor-capacitor design and its construction. It is validated experimentally with the theoretical parameters.
- **Chapter 3** discusses impedance control of the proposed component. Furthermore, the variable resistor controlled integrated inductor-capacitor equivalent is proposed and experimented with different load scenarios to compensate reactive power.
- **Chapter 4** further introduces a variable inductor controlled electrical equivalent of the integrated inductor-capacitor for reactive power compensation.
- **Chapter 5** shows the control of actual integrated inductor-capacitor using a variable inductor as a VAR compensator.
- Finally, **Chapter6** presents overall conclusions of all methods that have been developed. Some recommendations for future work in order to improve this performance are also given.

Chapter 2

Construction of an Integrated Inductor-Capacitor

This chapter gives an overview of the integrated inductor- capacitor devices available for low-and micro-power applications. It illustrates the basic construction of wound aluminum and polyester foils realized to obtain both inductance and capacitance in one by the particular positioning of the connection terminals of the foils. A detailed explanation of winding foils and determining the resulting RLC parameters is provided. The eventual construction of an integrated inductor- capacitor and its assessment by comparing measured and calculated parameters is undertaken.

2.1 State-of-the-Art

Diverse concepts and designs about the integration of inductors and capacitors constituting micro-and low-power components. It follows ongoing trend examining on this occasion in the present work possible medium and high power applications (Michael Casper, U.S. Patent 7,446,388 B29). Recent developments (Yuan, 2008) focus on the integration of capacitors, inductors, and resistors in thin film hybrid substrates suitable for RF/microwave, wireless, and optical transmission technologies. Cost effective constructions of integrated thin film inductor/capacitor are widely used in low power applications. Self-folding elastic electric devices presented (Miyashita et al., 2014) comprise integrated structures resistors, inductors and capacitors using metalized polyester films. This kinematic design, however, is restricted in its application, and therefore proposed by the authors mainly for sensors and actuators.

Chip implanted inductors in integrated component formation have drawbacks because of their low inductance values accompanied by quality factors in standard CMOS below 20 (Thanachayanont, 2000). Considering medium power application, a 5 kVA planar integrated inductor capacitor realized in

a transformer structure as part of a dc-dc medium power converter is presented in (Lembeye, Goubier, and Ferrieux, 2005). A further application of an integrated component is being realized in a harmonic filter for low and medium power systems presented in (Michaelides and Nicolaou, 2021).

The integration of capacitor and inductor into a single component is expected to reduce size, material, and consequently costs. Hence, design and construction of such integrated components, limited so far mainly to low and medium power applications, is of continuous interest to academia, thus promoting research towards higher power applications as well.

2.2 Concept

The integrated component destined to realize capacitance and inductance in one, is a reel of wound aluminum and polyester foils shown in Figure 2.1 as encountered in conventional foil wound capacitors.

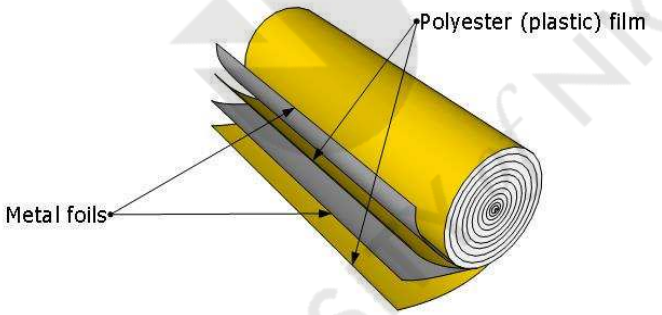

FIGURE 2.1: Wound foils yielding inductance and capacitance

The formation of the inductance resulting from the wound aluminum foils is being realized by the particular positioning of the connection leads along the length of the aluminum foils and the specific terminal operation (Michaelides and Nicolaou, 2017a). The four foils, two aluminum and two polyester, are shown unwound with the four contact terminals in Figure 2.2.

The supply terminals are placed at the opposite ends of two different foils while another two connection leads are placed on the remaining other two ends of the aluminum foils to serve as load terminals.

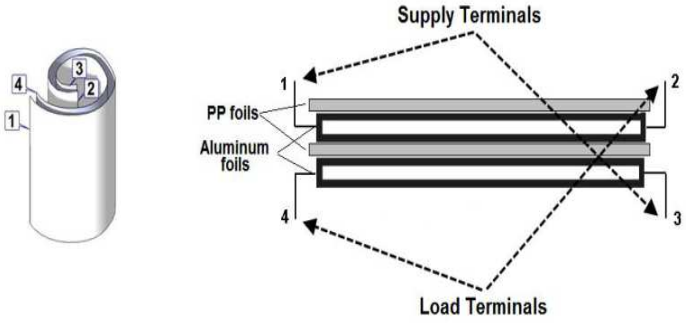

FIGURE 2.2: Unwound aluminum and polyester foils indicating terminal operation

2.3 Winding of Foils

Winding continuously the two aluminum and polyester foils as displayed in Figure 2.1 may realize any capacitance and inductance between the four ends of the two aluminum foils. However, the aluminum foils' resistance as it appears in the equivalent circuit in Figure 2.2 will be in acceptable high for big capacitance and inductance values because of the thin aluminum foils. As of this, the total foil length l_{Al} that is necessary to realize a certain capacitive reactive power is divided in n segments of equal lengths l_{seg} (Figure 2.3) which, in turn, are connected in parallel as shown in Figure 2.4.

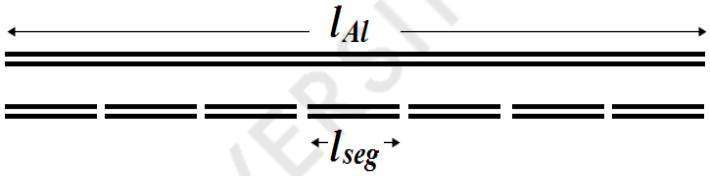

FIGURE 2.3: Aluminum foils of total length l_{Al} are divided in n equal segments of length l_{seg}

The division of the total foil length in n foil pieces (that is in the segments) will leave each segment with C/n capacitance. The parallel connection of the segments will restore the total initial capacitance C. The resistance of one segment will be smaller than that of the total foil length's resistance by the factor n. The parallel connection of n such segments will reduce the total foil length's resistance further by the factor n so that the resultant resistance of the component between the terminal 1-2 in Figure 2.4 is total foil length's resistance divided by n^2.

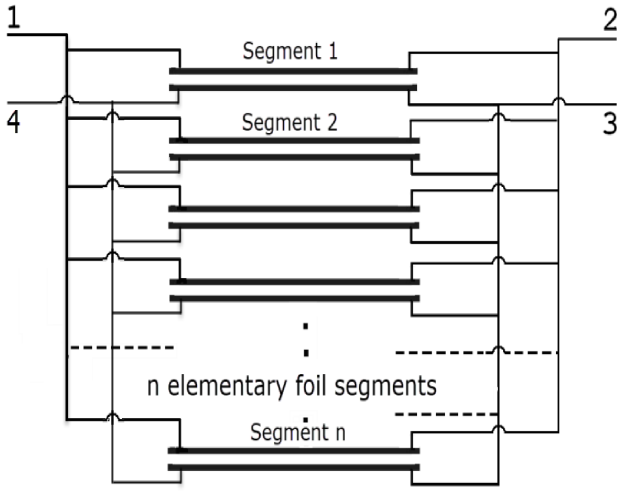

FIGURE 2.4: n foil segments connected in parallel

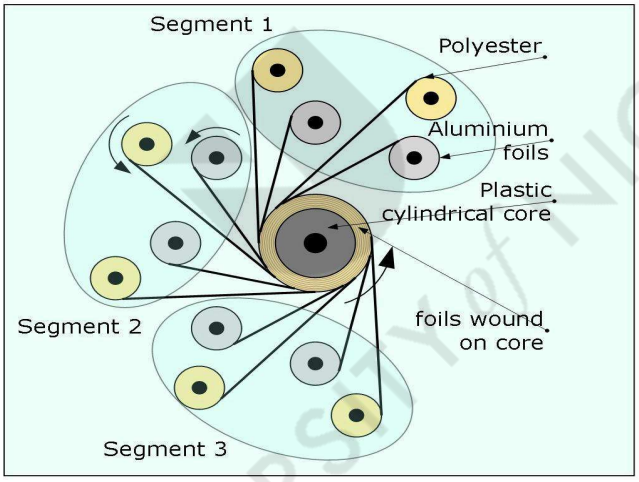

FIGURE 2.5: Three segments wound simultaneously

The inductance of a segment will be considerably smaller than that of the total foil's length because of the reduced length. Winding the segments separately one by one and connecting them in parallel as discrete components will reduce the inductance by the factor n as in the case of parallel resistors. Connecting the segments as discrete individual components will result to no improvement of the component's inductance quality factor.

The knowledge, however, that closely located inductors exhibit mutual inductance on each other, reconsiders the practice of treating the segments as discrete separate components but instead suggests their simultaneous winding on a same core. The coupling factor between two aluminum foils wound

simultaneously on the same core, because of their close and tight space arrangement, may be considered as one *k=1*. This means that the inductance of one segment when wound simultaneously on the same core with other n segments will increase by the factor n due to the mutual inductance exhibited by the other n segments. This increase of inductance of all n segments by the factor n counters the decrease of the resultant inductance due to parallel connection.

Hence, the significance of the integrated inductive capacitive component lies in the simultaneous winding of all aluminum foils as indicated in Figure 2.5 thus reducing the resistance while keeping the inductance constant realizing a quality factor of the component's inductance comparable to that of discrete component wire wound inductors.

2.4 Determining Technical Parameters RLC

A first orientation when designing the integrated inductor-capacitor component is the maximum expected reactive power that can provide. As of this for a desired capacitive reactive power Q_C and an operational voltage V, the capacitance is given in Equation 2.1.

$$C = \frac{Q_C}{V^2 \cdot 2\pi f} \tag{2.1}$$

The general equation of the capacitance of wound aluminum foils is given in Equation 2.2.

$$C = \frac{2 \cdot \varepsilon_o \varepsilon_r A}{d} \tag{2.2}$$

The area A is the aluminum foils length times width as shown in Figure 2.6 and d is the strength s_{pp} of the polyester foil. After substitution in Equation 2.2 we obtain Equation 2.3.

$$C = \frac{2 \cdot \varepsilon_o \varepsilon_r w_{Al} l_{Al}}{s_{pp}} \tag{2.3}$$

The capacitance C and geometric dimensions of the foils will determine via 2.3 the total length of the aluminum foils l_{Al} , an essential constructional parameter necessary to realize the desired capacitive reactive power Q_C. This will be followed by the determination of the segment's length l_{seg} that will realize the inductance L of the integrated component.

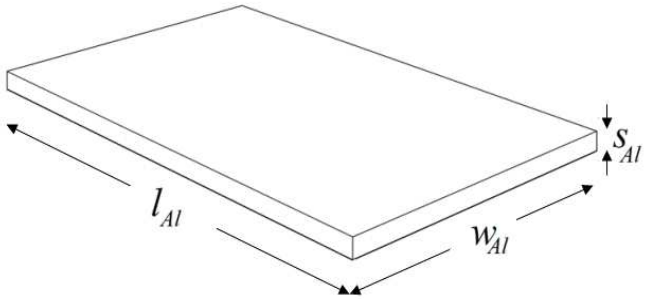

FIGURE 2.6: Dimension of aluminum foil

The general equation to calculate the inductance of a usual wire wound coil is given in Equation 2.4.

$$L = \frac{h \cdot N^2 \mu_0 A}{l} \tag{2.4}$$

As stated in (Reeves, 1978), considering the low grid frequency, a wire and foil wound inductor of the same number of turns and comparable size will have the same inductance.

Hence, Equation 2.4 shall be used in the present work to determine the segment's length l_{seg} of the wound foil component. The magnetic coupling of an inductor's windings, whether wire or foil wound, is always little less than one because of their spacing and different size, resulting to an increased value of the inductance in Equation 2.4. The Nagaoka Factor h is being introduced to counter this effect. The following two diagrams in Figure 2.7 show the determination of the Nagaoka factor as a function of the geometric dimensions of the component.

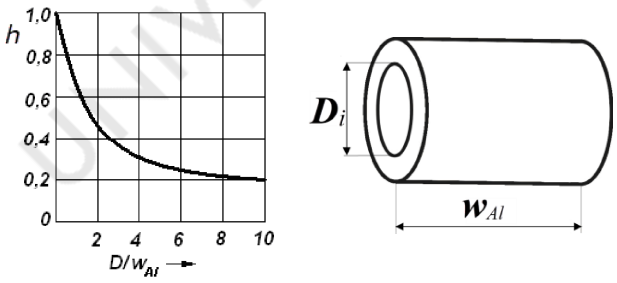

FIGURE 2.7: Dimensions of component with Nagaoka coefficient h

The circumference of the cylindrical component when multiplied with the number of foil turns N is the length of the foils, here defined as the length of

an elementary foil segment l_{seg}, resulting to Equation 2.5.

$$l_{seg} = \pi DN \tag{2.5}$$

The inductance of a foil segment l_{seg}, after substituting in Equation 2.4 the turns from Equation 2.5 and the cross-section $A = \pi\left({}^{D}/_{2}\right)^2$ becomes Equation 2.6.

$$L = h \cdot \left(\frac{l_{seg}}{\pi \cdot D}\right)^2 \frac{\mu_o}{w_{Al}} \cdot \pi\left(\frac{D}{2}\right)^2 \tag{2.6}$$

Simplifying Equation 2.6 with the permeability of free space $(\mu_o = 4\pi \cdot 10^{-7})$ Vs/Am results to Equation 2.7.

$$L = \frac{h \cdot {l_{seg}}^2 \cdot 10^{-7}}{w_{Al}} \tag{2.7}$$

Hence the length of the elementary wound foil segment l_{seg} becomes Equation 2.8 after rearranging Equation 2.7 with respect to l_{seg}.

$$l_{seg} = \sqrt{\frac{L \cdot w_{Al}}{h \cdot 10^{-7}}} \tag{2.8}$$

Eventually the above two lengths l_{Al} and l_{seg} determine the number of elementary foil segments that shall be wound simultaneously on the same core, connected in parallel as shown in Figure 2.4 and Figure 2.5. The total foil length l_{Al} is divided in pieces of segment's length l_{seg}. The ratio of the two latter lengths will determine the elementary segments n stated in Equation 2.9.

$$n = \frac{l_{Al}}{l_{seg}} \tag{2.9}$$

Rounding up of n always to the next bigger integer will influence preceding calculations of capacitance C and power Q insignificantly.

$$k^2 = \frac{4r_i \cdot r_j}{h_{i,j}^2 + \left(r_i + r_j\right)^2} \tag{2.10}$$

Considering the resistance of a conductor of length l, cross section A and a material resistivity ρ in Equation 2.11 results to an appropriate foil resistance for A = $W_{Al} \cdot S_{Al}$ shown in Equation 2.13, considering always the low grid frequency.

$$R = \frac{\rho \cdot l}{A} \tag{2.11}$$

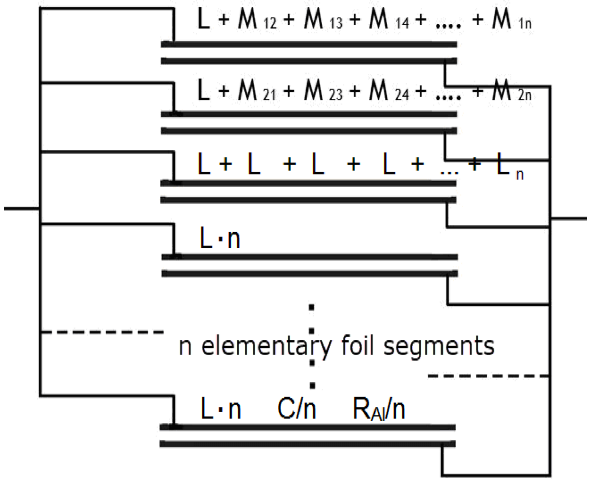

FIGURE 2.8: Mutual inductance occurred when all segments were connected in parallel

$$R_{foil} = \frac{\rho_{Al} \cdot l_{Al}}{w_{Al} \cdot S_{Al}} \tag{2.12}$$

$$R = \frac{R_{foil}}{n^2} \tag{2.13}$$

2.5 Winding of Pilot Model

The prospect of using such integrated inductor -capacitor in the grid as a VAR compensator considers essential the construction of a pilot model for appropriate experimentation. The model is designed to realize a power of 15 kVAR operating at 400 V, 50 Hz in the three phase power system. The parameters of the used materials for the construction of a pilot model are listed below in Table 2.1.

TABLE 2.1: Parameters of the Foils

Parameter	*Symbol*	*Value*
Aluminum foils width	W_{AL}	14cm
Aluminum foils strength	S_{AL}	4.4μm
Polyester foils strength	S_{pp}	6μm
Polyester foil dielectric	ε_r	2.5
Integrated component core diameter	D_i	19.5cm
Aluminum resistivity	ρ_{Al}	$2.65 * 10^{-8}$ Ωm

The initial parameter to lead via calculations to all other parameters is the maximum expected reactive power of the 15 kVAR component chosen here. Further, to achieve the dual property of the integrated component the ratio of capacitive to inductive reactance should be at least 6 : 1.

$$X_C : X_L = 6 : 1 \tag{2.14}$$

Using this ratio in equations Equation 2.14 and Equation 2.3 will yield a capacitance and inductance of C = 248 μF and L = 6.79 mH, respectively. Employing further Equation 2.7 will determine the necessary total aluminum foil length l_{Al} = 240 m and via 2.8 the segment's length l_{seg} =126 m. This means that the number of segments according to Equation 2.9 to be wound simultaneously following the proceeding analysis will be 240/126 =1.9 rounded up to the next integer $n = 2$. Calculating the resistance of a foil segment using Equation 2.12 results to a components resistance R=1.87 Ω. The constructional and technical parameters are listed in Table 2.2.

TABLE 2.2: Parameters of the Pilot Model

Pilot Model Parameters	*Calculated values*	*Measured values*
Capacitance C	248 μF	235 μF
Inductance L	6.79 mH	7.2 mH
Resistance R	1.87 Ω	1.76 Ω
Quality Factor Q	1.2	1.29
Total Length of the Foils	240 m	240 m
Length of Segment	126 m	126 m
Number of Segments	1.9	2

Polyester plastic foil has been used as a dielectric of the pilot model as it is practical for dry manual foil winding throughout experimentation.

To wind the foils, a mechanical arrangement of five rotating cylinders has been constructed as shown in Figure 2.9. Two cylinders hold the aluminum foil rolls, another two the polyester foil rolls, all four situated symmetrically around the central fifth cylinder on which the latter, two aluminum and two polyester foils shall be wound to form the integrated inductor-capacitor shown in Figure 2.10. Favorable for the winding process of the foils is the perfect parallelism of four foil rolls and their close distance to the middle component roll. The four foils are eventually wound on a plastic hollow pipe pushed on the middle wooden solid cylinder. The plastic pipe with the foils wound around it are shown on Figure 2.10.

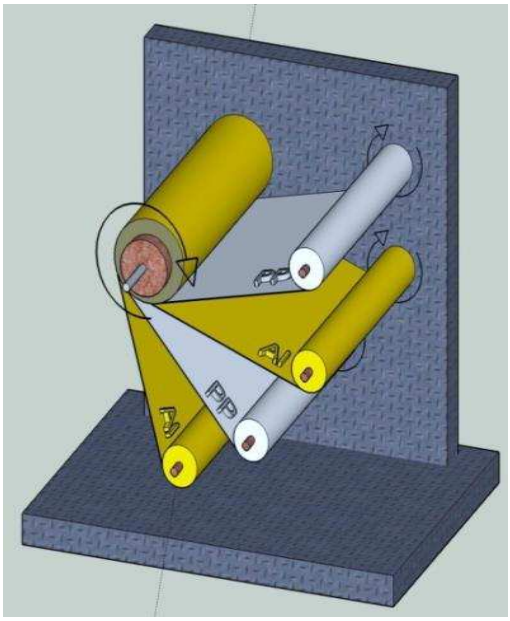

FIGURE 2.9: Winding mechanism

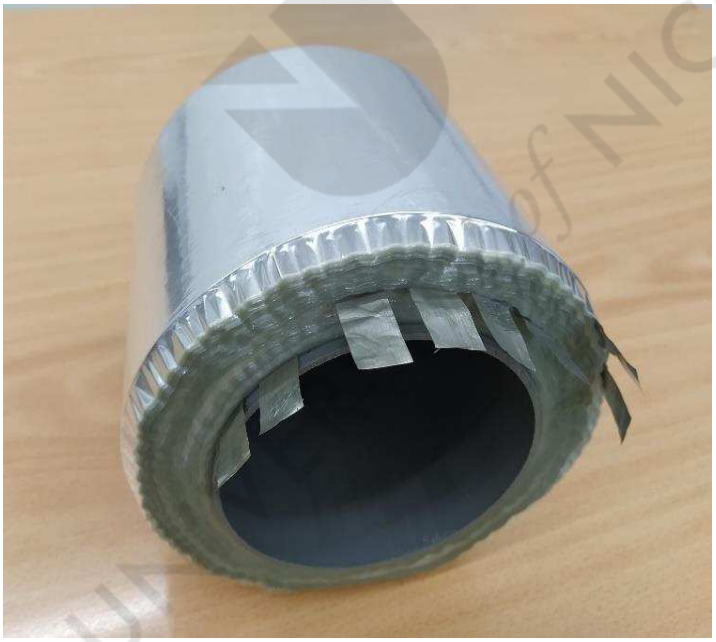

FIGURE 2.10: Integrated inductor-capacitor with terminal outlets/connections for measurement and operation of the component

It is pushed and fitted on a specially sized massive cylindrical wood supported on an axis between the two frame wooden walls. The axis is extended on the one side beyond the wall by a crankle which serves to turn the core. Manual winding of the foils while turning slowly the crankle is realized

amidst constant concern of wrinkling of the foils as they layer up. Wrinkling of the foils will disrupt the cylindrical shaped component and result to small air pockets between the foil layers causing a non-uniform electrical field and hence non uniform charge distribution throughout the foils. This way the four foils symmetrically arranged around the core roll at short distances and big angles to each other so that there is least contact between the foils while being pulled, wound around the core. This will avoid mutual attraction between the foils arising from electrostatic forces due to charging of the foils because of friction as they unwind from their rolls. At the present stage of the component's construction, a winding mechanism with n times four rolls as indicated in Figure 2.10 could not be realized to wind the segments simultaneously. Instead, the segments are wound one above the other. For a small number of segments implications are insignificant as the coupling factor between the different segments are still almost one.

The pilot model as it appears in Figure 2.10 is wound on a plastic hollow cylinder 18 cm long of diameter 12 cm. The inner diameter of the cylindrical wound foils is 12 cm and the outer is 18.2 cm. The mass of the component is 3.4 kg. The foils' dimensions are presented in Table 2.1. A reliable assessment about the calculation scheme and the construction of the pilot model is documented in Table 2.2 showing fair matching of calculated and measured values.

A reliable assessment about the calculation scheme and the construction of the pilot model is documented in Table 2.2 showing fair matching of calculated and measured values.

As the winding machine constructed for the occasion does not wind the foils as tight as industrial winding machines the measured capacitance of the pilot model is smaller than the calculated. The measured inductance of the pilot model is bigger than the calculated because the assumed component diameter is not the exact average diameter of the windings.

2.6 Discussion

In this chapter, the construction of the integrated device suitable to provide both capacitance and inductance in one component has been demonstrated. Further the developed calculation scheme has been verified via the measured technical parameters of the constructed pilot model. An indication for the success of exploiting a considerable inductance from the wound aluminum

foils, as a major challenge of this work, is the quality factor Q of the components inductance. The ratio of reactance to resistance of the component's inductance is according to the inductor's quality factor of Equation 2.15, $Q = 1.2$.

$$Q = \frac{\omega L}{R} \tag{2.15}$$

TABLE 2.3: Calculated parameters for different sizes

Q_C	Q_L	C(μF)	L(mH)	R(Ω)	l_{seg}	n	Q
15	15.6	248	6.8	1.87	126	1.9	1.2
25	26	414	4.1	0.67	98	4.1	1.9
30	31	497	3.4	0.47	89	5.4	2.3
35	36	580	2.9	0.34	82	6.8	2.6
40	41	663	2.5	0.26	77	8.3	3.1
45	46	746	2.2	0.20	72	9.9	3.4
50	52	829	2.1	0.16	70	11.6	3.9

Table 2.3 reveals a positive trend of the quality factor for components of higher power wound with more segments. As mentioned earlier the component is designed to realize for any size, equal capacitive as well as inductive reactive power documented in Table 2.3.

Chapter 3

Electrical Equivalent Circuit of Integrated Component

In this chapter, the wound aluminum and polyester foils are further examined in order to deduce the electrical equivalent circuit of the structure. This will be used in order to further quantitatively examine and investigate its properties and its suitability to act as a reactive power compensator. Implementing the structure through its equivalent circuit with only passive linear components, namely resistors, capacitors and inductors, allows us to improve the power factor while completely avoiding the increase of harmonic distortion generation.

3.1 Theory

An important step in order to analyze and understand the integrated component further is the derivation of its equivalent electric circuit. This equivalent circuit will enable the simulation of the wound foils structure by using linear, discrete components, namely resistors, capacitors and inductors, as shown in Figure 3.1, which are easily available in a variety of values in the market at reduced costs.

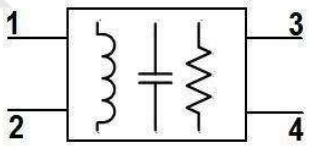

FIGURE 3.1: Four pole equivalent model consisting of RLC components

Appropriate to the four-terminal nature of the component through the two ends on each of its two aluminum foils as shown in chapter 2, Figure 2.2

, a four pole equivalent has been designed in (Michaelides and Nicolaou, 2017a) and will be used here.

In that work, the authors performed a number of measurements for a range of frequencies between the supply terminal pairs (1-3) while maintaining both open- and short-circuit on the load terminals (2-4). They observed that the behavior of the component was similar to series and parallel resonance circuits for wound conducting and insulating foils. This led to the two (extreme cases) operational modes (open- and short-circuit on load terminals) depicted in Figure 3.2.

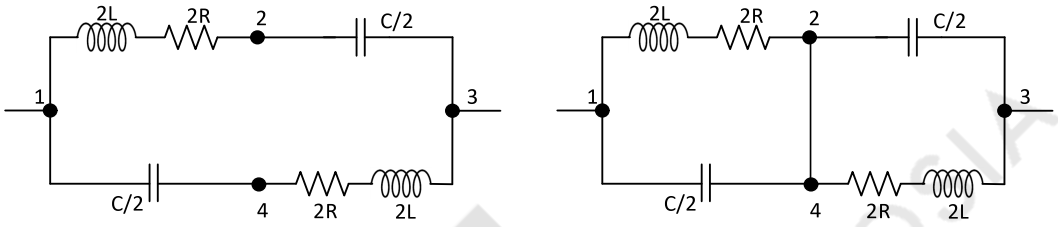

FIGURE 3.2: Four pole equivalent model for open load terminals and shorted load terminals

Observing the two versions, the authors therein realized that the only difference is the connection between the load terminals (2-4). Hence, they concluded that different impedance's connected across them, would realize the gradual transition of Z_{13} from one extreme to the other (i.e. from open-circuit to short-circuit). This is shown in Figure 3.3.

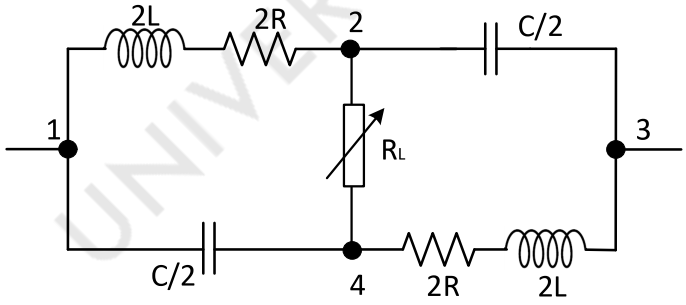

FIGURE 3.3: Components of equivalent and its nodes reflect the parameters of the aluminum foils and their four connection terminals respectively

The resistance R and the inductance L of the aluminum foils is measured using DC between terminals 1-2 or 3-4. The capacitance C is measured between terminals 1-4 or 2-3. All three values are the respective values shown in the equivalent circuit of Figure 3.3.

3.1.1 Calculating Z_{13}

To derive the impedance across terminals 1-3 (Z_{13}) one can choose elementary circuit theory on the equivalent circuit of Figure 3.3. This theory may involve wye-delta transformation or mesh analysis. Considering the circuit in Figure 3.4 and applying wye-delta transformation

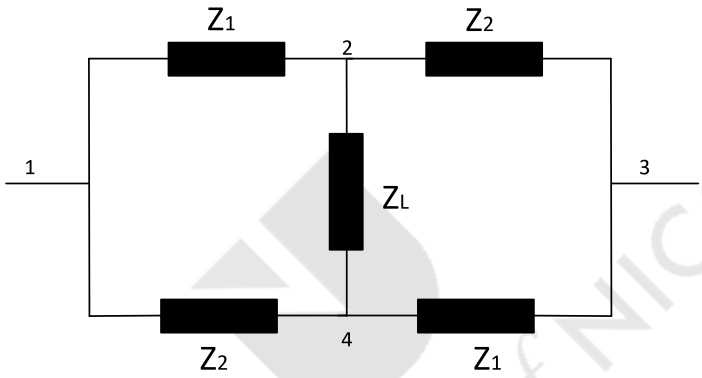

FIGURE 3.4: Equivalent circuit in terms of impedances

Applying Wye-Delta to Figure 3.4, then we get Figure 3.6

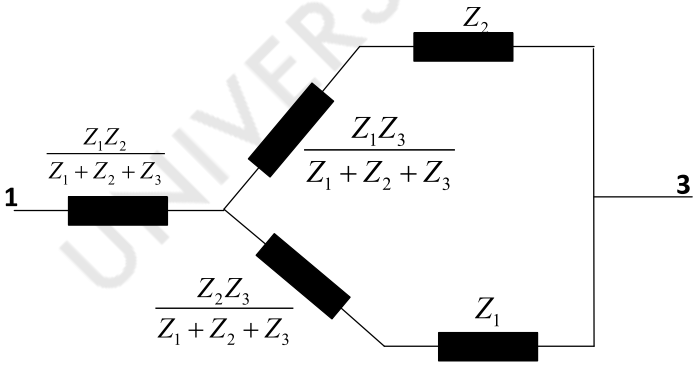

FIGURE 3.5: Star-delta transformations

Hence, then we get Figure 3.6

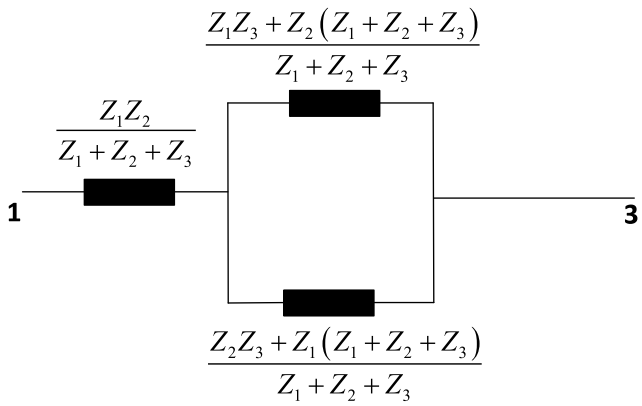

FIGURE 3.6: After series calculation

$$Z_{13} = \frac{Z_1Z_2}{Z_1 + Z_2 + Z_3} + \frac{[Z_1Z_3+Z_2(Z_1+Z_2+Z_3)][(Z_2Z_3+Z_1(Z_1+Z_2+Z_3))] \,/\, (Z_1+Z_2+Z_3)^2}{Z_1Z_3+Z_2(Z_1+Z_2+Z_3)+Z_2Z_3+Z_1(Z_1+Z_2+Z_3) \,/\, (Z_1+Z_2+Z_3)} \tag{3.1}$$

$$Z_{13} = \frac{Z_1Z_2}{Z_1 + Z_2 + Z_3} + \frac{Z_1Z_2Z_3^2 + Z_1^2Z_3\,(Z_1 + Z_2 + Z_3) + Z_2^2Z_3\,(Z_1 + Z_2 + Z_3)}{(Z_1 + Z_2 + Z_3)\,[(Z_1 + Z_2 + Z_3)\,(Z_1 + Z_2) + Z_3\,(Z_1 + Z_2)]} \tag{3.2}$$

$$Z_{13} = \frac{Z_1Z_2}{Z_1 + Z_2 + Z_3} + \frac{Z_1Z_2Z_3^2 + (Z_1 + Z_2 + Z_3)\left[Z_1^2Z_3 + Z_2^2Z_3 + Z_1Z_2\,(Z_1 + Z_2 + Z_3)\right]}{(Z_1 + Z_2 + Z_3)\,[(Z_1 + Z_2)\,(Z_1 + Z_2 + 2Z_3)]} \tag{3.3}$$

$$Z_{13} = \frac{Z_1Z_2}{Z_1 + Z_2 + Z_3} + \frac{Z_1Z_2Z_3^2 + (Z_1 + Z_2 + Z_3)\left[Z_1^2Z_3 + Z_2^2Z_3 + Z_1Z_2\,(Z_1 + Z_2 + Z_3)\right]}{(Z_1 + Z_2 + Z_3)\,[(Z_1 + Z_2)\,(Z_1 + Z_2 + 2Z_3)]} \tag{3.4}$$

$$Z_{13} = \frac{Z_1 Z_2 (Z_1 + Z_2)(Z_1 + Z_2 + 2Z_3) + Z_1 Z_2 Z_3^2 + (Z_1 + Z_2 + Z_3)\left[Z_1^2 Z_3 + Z_2^2 Z_3 + Z_1 Z_2 (Z_1 + Z_2 + Z_3)\right]}{(Z_1 + Z_2)(Z_1 + Z_2 + Z_3)(Z_1 + Z_2 + 2Z_3)} \tag{3.5}$$

$$Z_{13} = \frac{\left(Z_1^2 Z_2 + Z_1 Z_2^2\right)(Z_1 + Z_2 + 2Z_3) + Z_1 Z_2 Z_3^2 + (Z_1 + Z_2 + Z_3)\left[Z_1^2 Z_3 + Z_2^2 Z_3 + Z_1 Z_2 (Z_1 + Z_2 + Z_3)\right]}{(Z_1 + Z_2)(Z_1 + Z_2 + Z_3)(Z_1 + Z_2 + 2Z_3)} \tag{3.6}$$

$$Z_{13} = \frac{(Z_1 + Z_2 + Z_3)\left[Z_1^2 Z_2 + Z_1 Z_2^2 + Z_1^2 Z_3 + Z_2^2 Z_3 + Z_1 Z_2 (Z_1 + Z_2 + Z_3)\right] + \left[\left(Z_1^2 Z_2 + Z_1 Z_2^2\right) Z_3 + Z_1 Z_2 Z_3^2\right]}{(Z_1 + Z_2)(Z_1 + Z_2 + Z_3)(Z_1 + Z_2 + 2Z_3)} \tag{3.7}$$

$$Z_{13} = \frac{(Z_1 + Z_2 + Z_3)\left[Z_1^2 Z_2 + Z_1 Z_2^2 + Z_1^2 Z_3 + Z_2^2 Z_3 + Z_1 Z_2 (Z_1 + Z_2 + Z_3)\right] + Z_1 Z_2 Z_3 (Z_1 + Z_2 + Z_3)}{(Z_1 + Z_2)(Z_1 + Z_2 + Z_3)(Z_1 + Z_2 + 2Z_3)} \tag{3.8}$$

$$Z_{13} = \frac{\left[2Z_1^2 Z_2 + 2Z_1 Z_2^2 + Z_1^2 Z_3 + Z_2^2 Z_3 + 2Z_1 Z_2 Z_3\right]}{(Z_1 + Z_2)(Z_1 + Z_2 + 2Z_3)} \tag{3.9}$$

$$Z_{13} = \frac{2Z_1 Z_2 (Z_1 + Z_2) + Z_3\left(Z_1^2 + Z_2^2 + 2Z_1 Z_2\right)}{(Z_1 + Z_2)(Z_1 + Z_2 + 2Z_3)} \tag{3.10}$$

$$Z_{13} = \frac{(Z_1 + Z_2)\left[2Z_1 Z_2 + (Z_1 + Z_2) Z_3\right]}{(Z_1 + Z_2)(Z_1 + Z_2 + 2Z_3)} \tag{3.11}$$

$$Z_{13} = \frac{\left[2Z_1 Z_2 + (Z_1 + Z_2) Z_3\right]}{(Z_1 + Z_2 + 2Z_3)} \tag{3.12}$$

Substituting $Z_1 = 2R + 2j\omega L$, $Z_2 = {}^{-2j}/_{\omega C}$, $Z_3 = R_L$ in Equation 3.12 we get Equation 3.13

$$Z_{13} = \frac{\left[(4R + 4j\omega L)\left(\frac{-2j}{\omega C}\right)\right] + \left(2R + 2j\omega L - \frac{2j}{\omega C}\right)}{2R + 2j\omega L - \frac{2j}{\omega C} + 2R_L} \tag{3.13}$$

$$Z_{13} = \frac{\left(\frac{-2j}{\omega C}\right)[(4R + 4j\omega L)] + \left(\frac{2\omega RC + 2j\omega^2 LC - 2j}{\omega C}\right) R_L}{\left(\frac{-2j}{\omega C}\right)[j\omega RC + j\omega R_L RC - \omega^2 LC + 1]} \tag{3.14}$$

$$Z_{13} = \frac{4R + 4j\omega L + j\omega RC \cdot R_L + R_L\left(1 - \omega^2 LC\right)}{j\omega C\left(R + R_L\right) + 1 - \omega^2 LC} \tag{3.15}$$

It follows, therefore, that the impedance across terminals 1-3 is given by Equation 3.15.

3.2 Determining the Circuit's Power

Winding the foils for an integrated component to exhibit the widest range of impedances that span from an extreme capacitive to an extreme inductive value is quite a complicated process that utilizes specific winding equipment and requires materials of different sizes. Such an approach is, thus, well beyond the scope of the current work. The importance of using the equivalent circuit of the component is that it allows one to easily express the impedance Z_{13} as a mere function of the structure's technical parameters (R, L and C), the operating frequency ω, and the load terminal impedance R_L.

A significant design parameter is the maximum reactive component the device is expected to compensate, that is, the reactive power it is capable of absorbing or injecting to the network for power factor compensation. This reactive power leads to the choice of the discrete components to be used in the equivalent circuit.

For instance, to compensate a 240V single-phase 350W induction motor with a nominal power factor of 0.75, the component should be able to inject reactive power of

$$Q_{compensation} = \tan(\cos^{-1}(PF)) \times P_{motor} = \tan(\cos^{-1}(0.75)) \times 350 = 308.67\,\text{VAR} \tag{3.16}$$

Furthermore, to achieve the dual (capacitive and inductive) character of the circuit, it is intuitive that the ratio of capacitor to inductor reactance should be well beyond 10, that is

$$\left|\frac{X_C}{X_L}\right| = \left|\frac{1}{\omega^2 LC}\right| >> 10 \tag{3.17}$$

(the reason will become apparent in the following paragraphs). In this work the ratio is chosen to be around 13.

From Equation 3.15 of Z_{13} , it is easily understood that the component can provide maximum capacitive and maximum inductive compensation when the load impedance R_L is at either one of two extremes: open circuit for maximum capacitive character (when we are forcing the current through the capacitors), and short circuit for maximum inductive character (when almost all current passes through the inductors). Under these fixed operational modes Z_{13} becomes Equation 3.18 and Equation 3.19

$$Z_{13}(\max capacitive) = \frac{1 + j\omega C\,(\omega L - R)}{j\omega C} \tag{3.18}$$

R_L open-circuit, the circuit essentially reduces to two parallel branches made of a resistor-inductor-capacitor in series.

$$Z_{13}(\max\ inductive) = \frac{4j\omega L + 4R}{j\omega CR + 1 - \omega^2 LC} \tag{3.19}$$

R_L short-circuit - substituting R_L = 0 in Z_{13} equation

Considering the above, for the aforementioned 350W domestic motor scenario, two 10 μF capacitors and two 80mH inductors (with internal winding resistance of 5 Ω) can be chosen, both of which can be easily found in the market. These components translate to R = 2.5 Ω, L= 40 mH and C = 5 μF in the equivalent circuit. The load resistor can be realized with a 1 $k\Omega$ variable resistor. Note at this point that these values are consistent with the previous remark on the capacitor to inductor reactance ratio as, at 50 Hz, they produce a ratio of almost 13 (12.66).

Figure 3.7 shows the real and imaginary parts of Z_{13} as a function of the chosen parameters and frequency of 50Hz. From the figure it is easily understood that $R_L \approx 84\ \Omega$ is the point where the component is neutral (purely resistive), so below that it exhibits an inductive character and above that a capacitive character.

The expected compensation of the component is realized by the reactive power it produces

$$Qcompensation = \mathrm{Im}\left\{\frac{240^2}{Z_{13}}\right\} \tag{3.20}$$

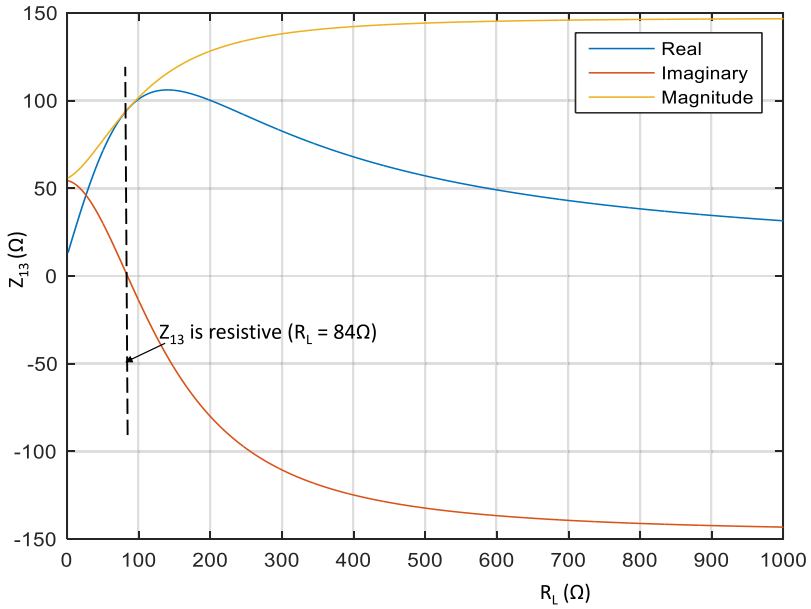

FIGURE 3.7: Real and imaginary parts of Z_{13} when C=20 μF, L=40 mH, R=2.5 Ω and R_L varies from 1 Ω to $k\Omega$

When plugged in the equations, the above component values are expected to slightly overcompensate the lagging phase of the 350W induction motor when R_L is open-circuit by injecting 390 VAR to the network. At the other fixed operational mode (when R_L is short circuit), the component is rendered inductive as almost all of the current flows through the inductors and is expected to absorb 1,012 VAR. When R_L is 84 Ω (neutral point), no reactive power is exchanged with the network. These points are graphically depicted in Figure 3.8.

Using these values, the equivalent circuit becomes as in Figure 3.9. To have almost all current through the inductors under short circuit across terminal load impedance is exactly the reason why we need to maintain a high capacitive to inductive reactance ratio. Remember that in this work we chose a ration of 12.66:1.

3.3 Calculations

3.3.1 Capacitive Load

First we simulate a capacitive load using a 60 Ω resistor in parallel with a 40 μF capacitor, as shown in Figure 3.10 with connecting the equivalent circuit.

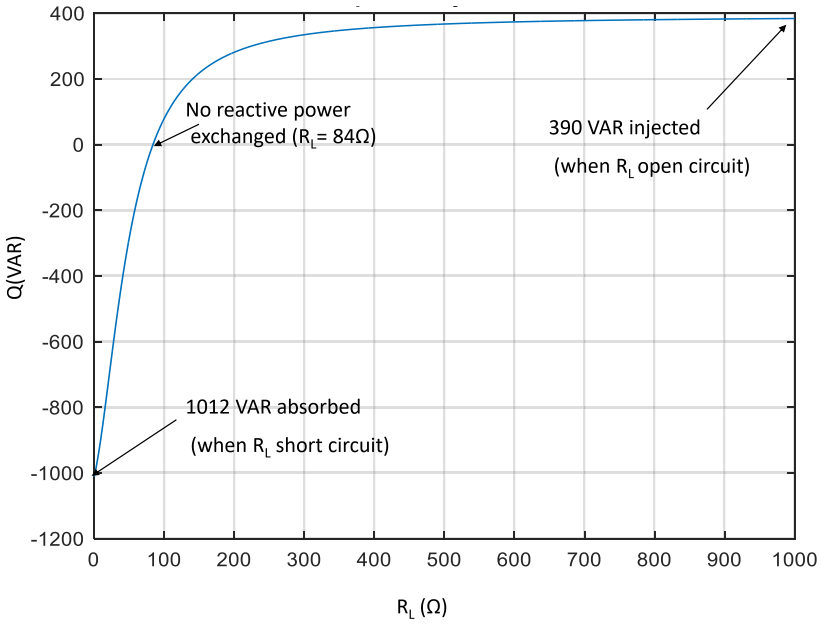

FIGURE 3.8: Reactive power compensation for the discrete component values chosen

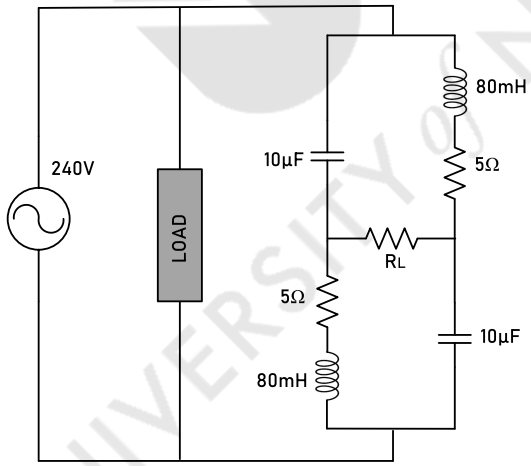

FIGURE 3.9: Circuit destined to compensate reactive power via adjustment of R_L

The capacitor impedance is $Z_C = 1/j\omega C = -80\Omega$.
This capacitive load injects reactive power of

$$X_{Cap.load} = \text{Im}\left\{\frac{V_S^2}{\frac{1}{j\omega C}}\right\} \simeq 720\,\text{VAR} \tag{3.21}$$

The phase ϕ and current I_L are calculated from the currents I_R and I_C.

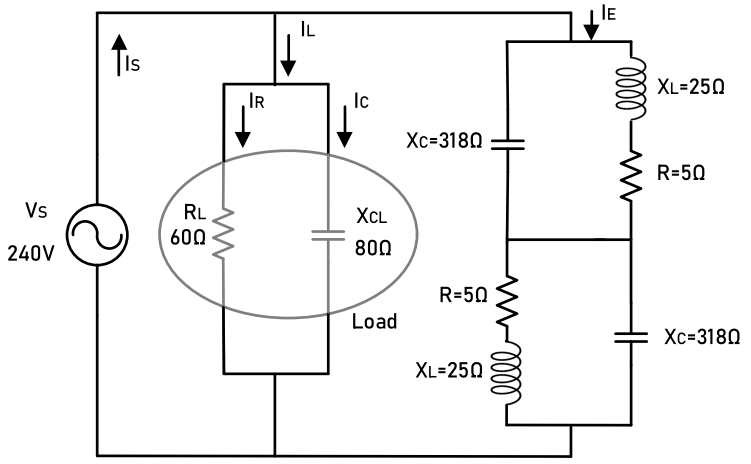

FIGURE 3.10: Load terminals of circuit shorted so that latter can provide inductive reactive power to compensate capacitive reactive power of load

The current through the resistor is given by
$I_R = 240\text{V}\angle 0°/60\Omega\ \angle 0° = 4\text{A}\angle 0°$.

The current through the capacitor is given by
$I_C = 240\text{V}\angle 0°/80\Omega\angle 90° = 3\text{A}\angle 90°$.

Using these currents, one can easily get the phase ϕ_{I_S} and magnitude $|I_S|$ of the source current using $|\phi_{I_S}| = \sqrt{(I_R)^2 + (I_C)^2} = 37°$ and $|I_L| = 5$ A.

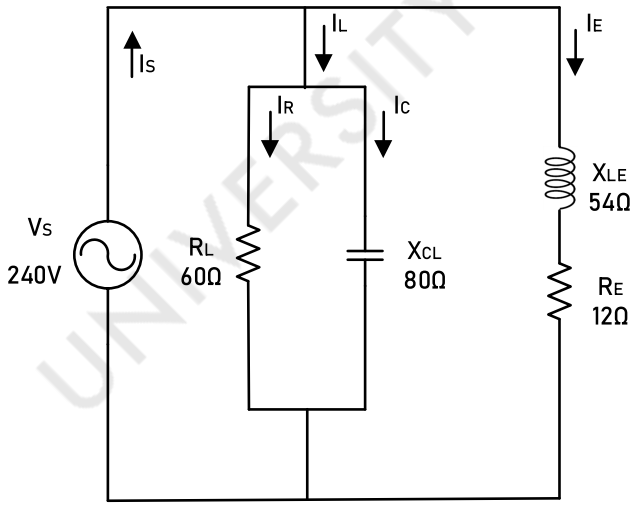

FIGURE 3.11: Circuit with shorted load terminals reduced to series R_L configuration

To employ compensation, the equivalent circuit is connected in parallel to the capacitive load maintaining a short circuit across terminal impedance R_L

for maximum reactive power absorption. As previously stated, under short circuit operational mode the equivalent circuit is capable of absorbing 1012 VAR of reactive power, thus overcompensating the capacitive load. Under R_L short circuit, the equivalent circuit can be simplified by the series addition of the two parallel LC configurations to yield the *RL* branch shown in Figure 3.11.

TABLE 3.1: Calculations when system is loaded with capacitor

System Parameters	*Not Compensated*	*Partially Compensated*	*Fully Compensated*
Active Power P (W)	960	1180	1056
Reactive Power Q (VAR)	-720	294	0
Phase ϕ (^{o})	37	-14	0
System Current I_S (A)	5	5.1	4.4
Equivalent Current I_E (A)	-	4.33	3.3
Load resistor R (Ω)	-	0	20

Again, this is due to the capacitor to inductor reactance ratio as mentioned earlier (maintaining this ratio high forces most of the current through the inductors, rendering the capacitor branches as almost open circuits and minimizing their impact). At this point it is helpful to gain a view of the phasor diagram of the whole arrangement. This is presented in Figure 3.12 . In the diagram, V_s is the supply voltage, I_C the -80 Ω capacitor current, IR the 60 Ω resistor current and I_E is the current through the equivalent circuit. As it can be observed in the diagram, I_E can be further broken into its constituent components, namely the reactive current I_{Ei} and the active (resistive) current I_{Er} which result from its phase with V_s (denoted as ϕ_1).

It follows that the active system current I_r is the addition of the active current through the capacitive load and the active current through the equivalent circuit $I_r = I_R + I_{Er}$

Similarly, the system reactive current I_i is the addiction of the reactive currents through the capacitive load and the equivalent impedance $I_i = I_C + I_{Ei}$.

Using the specific discrete component values introduced earlier, the equivalent impedance becomes $Z_E = 12 + j54\ \Omega$, which yields a current magnitude $|I_E| = 240\ V/\sqrt{(12^2 + 54^2)} = 4.33$ A and current phase $\phi_1 = tan^{-1}\ (54\ /\ 12)$ =77.5, so the equivalent circuit current becomes $I_E = 4.33\ A\ \angle 77.5°$.

It follows, then, that the active equivalent current component is given by $I_{Er} = I_E \cdot \cos\phi_1 = 0.94A$ (in phase with system voltage), while its reactive component is $I_{Ei} = I_E \cdot \sin\phi_1\ \angle -90° = 4.23\ A \angle -90°$

Combining the above, we can get the system current active component I_r = 4+0.94 A (in phase with the system voltage), and the system current reactive component by Ii = 3A$\angle 90°$ + 4.23A$\angle -90°$.

Substituting now the final component currents of the system I_r and I_i in ϕ = $tan^{-1}(I_i/I_r)$ and $|I_S|$ = $\sqrt{(I_r^2 + I_i^2)}$ provides the phase and system current as Is = 5.09A$\angle -14°$ A. The above suggest that when the equivalent circuit is employed at its maximum absorbing capability (terminal load resistance short circuit) it slightly overcompensates the capacitive load reactive power by reducing it from 37° to $-14°$.

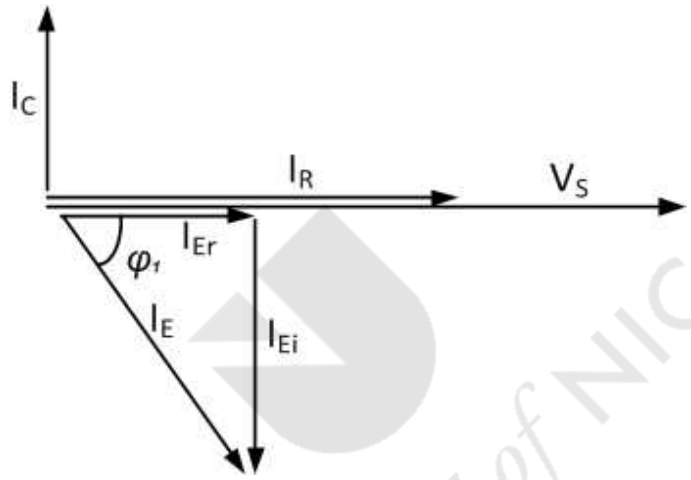

FIGURE 3.12: Voltage and currents of the system in vector presentation

Targeting complete compensation translates to canceling all reactive current in the system. Observing the phasor diagram of Figure 3.11, this means regulating the reactive current in the equivalent circuit I_{Ei} to the same magnitude as I_C .

The impedance of the equivalent circuit Z_{13} for any value of terminal load resistance R_L was presented in Equation 3.15. Rearranging that equation to rectangular form allows us to express the impedance of the equivalent in the form Z_E = a + jb revealing, thus, its real and imaginary parts. Following this path, the current of the equivalent $I_E = |I_E|\angle\phi_1$ becomes $|I_E| = V_S/\sqrt{a^2 + b^2}$ and the phase $\phi_1 = tan^{-1}(b/a)$. Similarly, the reactive component of the current I_E becomes $I_{Ei} = |I_E| \cdot sin\phi_1$. For complete cancellation, i.e. to achieve zero phase, we need to equate I_C to I_{Ei} which leads to:

$$3 - \left({}^{240}/_{\sqrt{(a^2+b^2)}\cdot\sin\left(\tan^{-1}(b/a)\right)} \right) = 0 \tag{3.22}$$

which is a transcendental equation and requires numerical methods to solve. Using Matlab the above yields $R_L = 20\Omega$. This is the resistance that has to be adjusted at the load terminals of the equivalent circuit to achieve zero phase in the system between voltage V_S and current I_S.

3.3.2 Inductive Load

As mentioned earlier, a domestic single phase 350W induction motor operating at PF=0.75 can serve as an inductive load. The motor's PF = 0.75 yields a displacement angle $\phi = 41.4°$ between the system's voltage and current. In theory, this can be realized simply with a parallel configuration of a 164 Ω resistor in with a 594 mH ideal inductor, as presented in Figure 3.13. The corresponding phasor diagram (without the equivalent circuit involved) can be seen in Figure 3.14 .

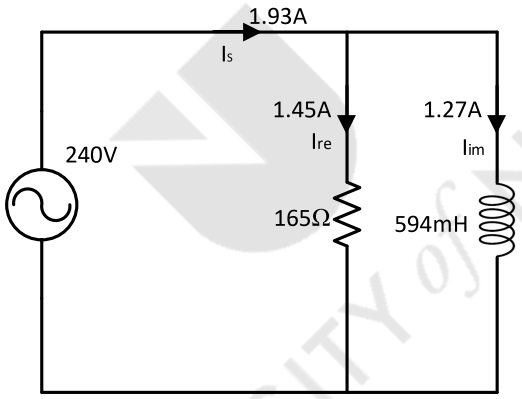

FIGURE 3.13: Simplified motor equivalent presented by resistor and inductor

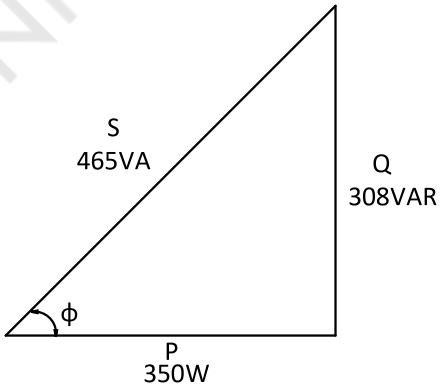

FIGURE 3.14: Power triangle of motor

The active current through the motor is given by $I_{re} = 240\angle 0 / 186.5\angle 90 = 1.27\angle -90°$ A.

The active current through the motor is given by $I_{im} = 350W/240 \cdot cos41.4° = 1.93$ A.

As before, the component equivalent circuit is then connected in parallel to the motor as shown in Figure 3.14, now having its terminal load resistance open circuit for maximum reactive power injection.

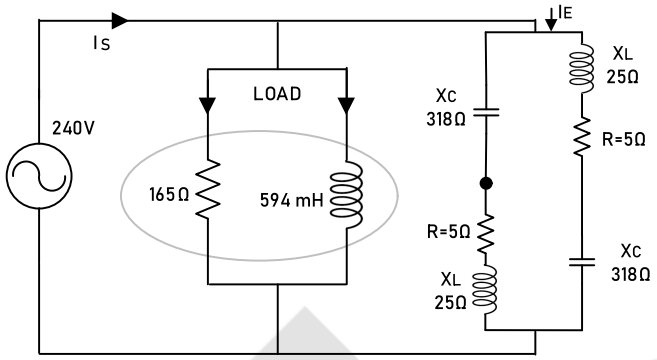

FIGURE 3.15: Equivalent circuit with open-load terminals providing thus maximum capacitive reactive power destined to compensate inductive reactive power of the motor

Under this extreme operational mode (Figure 3.16), the equivalent circuit produces an almost purely capacitive impedance (angle is calculated at $-89°$), however, using the 1 kΩ variable resistor at its maximum we get an angle of $-77.6°$ (Figure 3.17), which corresponds to the 390 VAR reactive power injection. As stated earlier, this slightly overcompensates the motor as full compensation requires only 308.67 VAR.

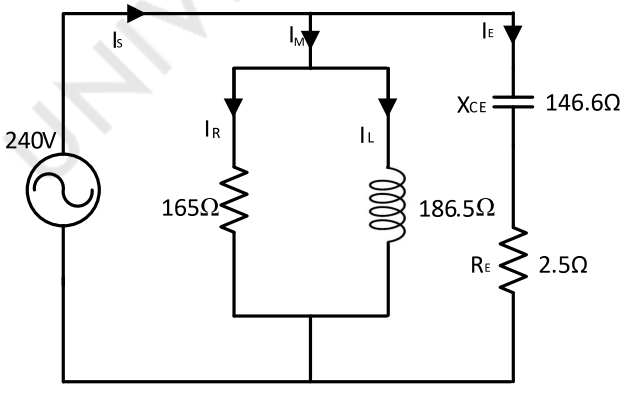

FIGURE 3.16: Circuit with open load terminals simplified to series capacitive resistive connection

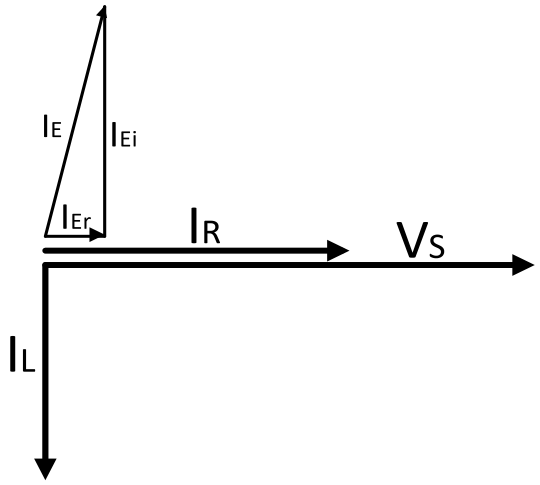

FIGURE 3.17: Phasor presentation of motor and circuit currents and voltages.

The system active current is obtained by $I_r = I_R + I_{Er}$, and the system reactive current by $I_i = I_L + I_{Ei}$. Z_{13} when R_L is open-circuit is $Z_{Eo} = 2.5 - j146.6$.

The current through the component equivalent circuit is given by $|I_E| = 240V/\sqrt{2.5^2 + 146.6^2}\Omega$ and $\phi_2 = tan^{-1}(146.6/2.5)$ resulting to $I_E = 1.63A\angle 89°$

It follows $|I_{Er}| = I_E \cdot cos\phi_2$ that is $I_{Er} = 0.028A\angle 0°$.

$|I_{Ei}| = I_E \cdot sin\phi_2$ that is $I_{Ei} = 1.62A\angle 90°$.

$I_i = 1.2A\angle -90° + 1.62A\angle 90°$

$I_r = 1.45A\angle 0° + 0.11A\angle 0°$

Substituting now the final component currents of the system I_r and I_i in $\phi_2 = tan_{-1}(I_i/I_r)$ and $|I_S| = \sqrt{I_r^2 + I_i^2}$ provides the phase and current of the system $\phi_2 = -14°$ and $|I_S| = 1.5A$.

Equating, as before, the magnitudes of the reactive currents through the equivalent circuit and the motor for complete compensation, i.e. using and solving the transcendental Equation 3.22, yields terminal load resistance of 239Ω.

TABLE 3.2: Calculations of the system when loaded with an induction motor

System Parameters	*Not Compensated*	*Partially Compensated*	*Fully Compensated*
Active Power P (W)	352	362	530
Reactive Power Q (VAR)	310	-83	0
Phase ϕ (^{o})	-41	13	0
System Current I_S (A)	1.95	1.55	2.2
Equivalent Current I_E (A)	-	1.68	3.32
Load resistor R (Ω)	-	∞	238

3.4 Measurements

In order to verify the preceding analysis, an experimental setup was used in order to measure the ability of the component's equivalent circuit to compensate reactive power. The experiments were conducted in the laboratory on the 240V, low voltage grid supply. The discrete component values of the equivalent circuit were the ones discussed in the previous section.

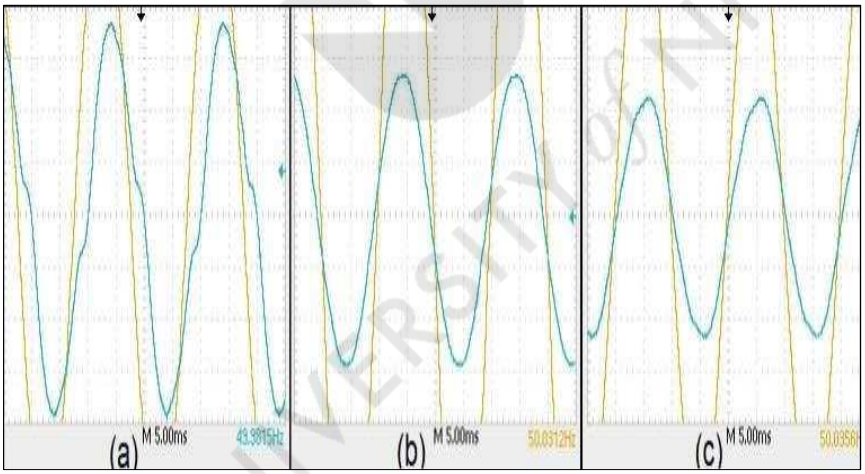

FIGURE 3.18: Phase between voltage and current when system is loaded with capacitive load, a) no compensation is attempted, b) moderated compensation is applied, c) complete compensation is achieved

First, the circuit of Figure 3.10 was realized using a parallel RC configuration. Figure 3.18(a) presents the system voltage (yellow) and current (green) prior to the equivalent circuits involvement. From that figure, it is easily observed that the current is leading the voltage by 39°. Table 3.3 presents the system current (in this case, same as load current) magnitude at 5.1 A. After

connecting the equivalent circuit with its load terminals short-circuited, and as expected and stated in the preceding analysis, we observe an overcompensation on the system, thus creating a lagging current. This is depicted in Figure 3.18(b) where the current lies slightly (by around 16°) to the right of the voltage. Connecting and fine-tuning the variable resistor across the load terminals, we observe that the displacement power factor is completely eliminated at R_L = 18 Ω. This is shown in Figure 3.18(c) and is in excellent agreement with the above theoretical analysis which expected the elimination to occur at R_L = 20 Ω.

TABLE 3.3: Measurements in the system when loaded with a capacitor

System Parameters	*Not Compensated*	*Partially Compensated*	*Fully Compensated*
Active Power P (W)	952	1200	1090
Reactive Power Q (VAR)	-770	344	0
Phase ϕ (^{o})	39	-16	0
System Current I_S (A)	5.1	5.2	4.55
Equivalent Current I_E (A) -	-	4.41	3.3
Load resistor R (Ω)	-	0	18

Furthering the experimentation, the possibility of having the component equivalent to compensate the phase lag caused by an induction motor was also examined. As previously stated, this inductive load comes in the form of a single 350 W phase induction motor with PF at 0.75. The same setup as above is used. When initially the component is not involved, the motor draws a current of 1 A. The power triangle of the motor is shown in Figure 3.14 The current the motor draws is 1.9 A with a lagging angle of 41.4°.

TABLE 3.4: Measurements of the system when loaded with an induction motor

System Parameters	*Not Compensated*	*Partially Compensated*	*Fully Compensated*
Active Power P (W)	332	377	552
Reactive Power Q (VAR)	309	-80	0
Phase ϕ (^{o})	13	-12	0
System Current I_S (A)	1.89	1.61	2.3
Equivalent Current I_E (A)	-	1.72	3.25
Load resistor R (Ω)	-	∞	240

Figure 3.19(a) shows the oscilloscope waveforms for the current (green) and voltage (yellow), with an angle of 43°, which is acceptably close to the

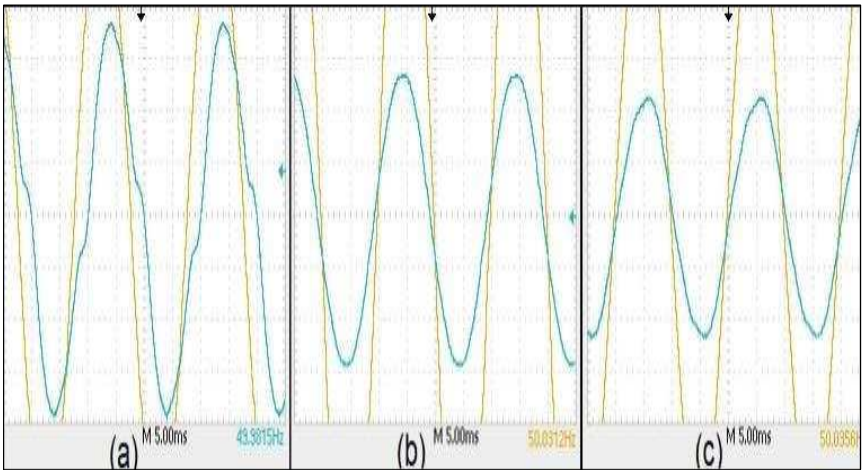

FIGURE 3.19: Phase between voltage and current when system is loaded with an induction motor a) no compensation is attempted b) moderated compensation is applied c) complete compensation is achieved

calculated 41.4°. When the component equivalent circuit is connected (with its load terminals open-circuit for max reactive injection), an overcompensation is observed, as in Figure 3.19(b). Current therein leads voltage by 13°, which again is very close to the calculated 14°. As before, connecting the variable resistor across the load terminals and fine-tuning it, we were able to eliminate the phase between the current and voltage as in Figure 3.19(c). The observed experimental R_L value to achieve that was recorded at R_L=240 Ω.

3.5 Discussion

In this chapter we examined the behavior of the integrated component using its equivalent circuit, which is constructed exclusively by linear discrete components and was initially derived in (Michaelides and Nicolaou, 2017a). The theoretical analysis and calculations demonstrated how the component can be sized to compensate a range of both capacitive and inductive displacement power factors simply by fine tuning its terminal load impedance (in this case resistance, R_L). Laboratory experiments were also carried out to verify the calculations and the prospect of using the component equivalent circuit to compensate reactive power. During these experiments both capacitive and inductive loads were considered, producing a displacement angle between the load current and voltage. Connecting the equivalent circuit in parallel to the loads, we were able to successfully eliminate any displacement

between system current and voltage. All experimental measurements were tabulated and compared to the theoretical calculation results. The fact that the two were found in excellent agreement suggests that the component is indeed suitable for regulating smoothly both leading and lagging phase angles between system voltage and current and, since this is achieved using only linear electrical components, without generating unwanted harmonic distortion. However observing on Table 3.4 the relative high active power mainly converted the adjustable resistor requires qualified consideration to reduce the losses. A first attempt to realize the latter is the employment of a variable inductor instead. Calculations show that the variable inductor connected at the load terminals of the circuit may change equally accurate the terminal impedance between terminals 1-3 of the equivalent circuit. Employing power electronics for the regulation of the current between the load terminals 2-4 is not being considered as the latter practice will result to harmonic modulation. Hence, an air wound inductor will be further examined to see if it maintains linearity.

Chapter 4

Control of Electrical Equivalent Circuit

This chapter introduces a variable inductor to control the wound aluminum and polyester foils equivalent circuit. This variable inductor functions on the principle of mutual inductance and hence avoids the employment of power electronics to realize variable inductance. The proposed inductor is designed to be varied automatically and thus provide extended automatic regulation of the electric circuit's impedance.

4.1 Concept

The impedance Z_{13} destined to control the terminal impedance of the circuit (Chapter 3, Figure 3.3) is being realized in this case by a variable inductor Z_C shown in Figure 4.1. The gradual inductance change of the variable inductor avoids abrupt current changes during the control process and consequently the creation of harmonics through the employment of power electronics. Conventional analysis (Yuan, 2008) of the circuit as shown early above yields chapter 3, Equation 3.15 where the impedance Z_C represents the reactance of the variable inductor in 4.1 leads to its terminal impedance Z_{13} as shown below in Equation 4.1.

The possibility to operate the circuit with a capacitive as well as inductive terminal impedance shall be examined by constructing the circuit with discrete components namely two 10 μF and two 80 mH air-wound inductors with a wire resistance 5 Ω. Altering the terminal impedance Z_C of the circuit will be attempted via the air wound variable inductor connected at the load terminals 2-4.

$$Z_{13} = \frac{2j\omega L + 2R + j\omega RC \cdot Z_C + Z_C\left(1 - \omega^2 LC\right)}{j\omega 2C\left(\frac{R}{2} + Z_C\right) + 1 - \omega^2 LC} \tag{4.1}$$

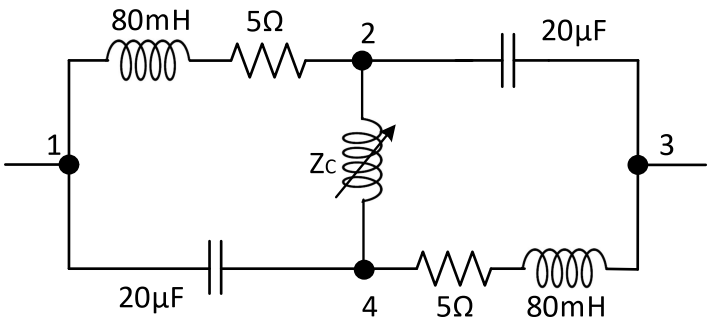

FIGURE 4.1: Regulating the terminal impedance of the circuit via an adjustable inductor

4.2 Variable Inductor

The variable inductor functions on mutual inductance principle. It consists of two round cylindrical separate inductors of different diameters connected in series. For maximum mutual magnetic linkage, the smaller inductor is mounted on a stepper motor directly inside in the middle of the big inductor as shown in Figure 4.2. The magnetic fields of the two inductors will reinforce when the two inductors are aligned co-axially in one direction resulting to a maximum inductance. When the inner inductor is turned via a stepper motor in opposite direction, that is 180°, the magnetic fields oppose each other thus reducing the effective inductance of the pair to a minimum. To suit the values of the circuit's components (that is two capacitors and two inductors), the variable inductor is especially designed to range from 150 mH to 270 mH. For lowest inductance, 150 mH the circuit provides maximum capacitive reactive power and for the inductance of 270 mH a maximum inductive reactive power respectively. An inductance at mid-range of the variable inductor, that is 220 mH, will turn the impedance of the circuit neutral reactive that is purely active with high resistance.

4.3 Calculations

The terminal impedance of the circuit Z_{13} as a function of variable inductor's value is presented by its changing magnitude/phase shown in Figure 4.3. The left function reveals a clear inductive phase for small values of the variable inductor and a capacitive phase for big values, respectively. Zero phase occurs at mid range of the variable inductor 210mH at which the circuit does not provide/consume any reactive power to/from the grid.

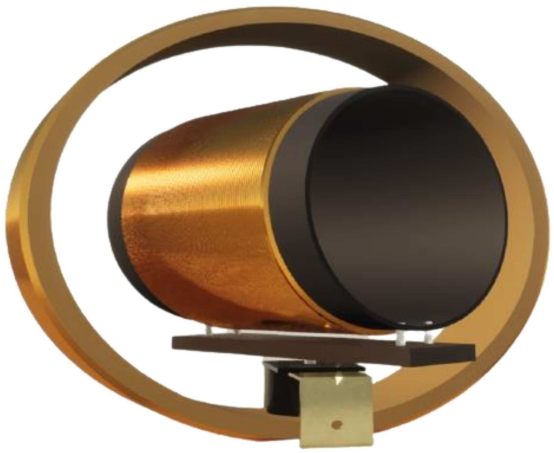

FIGURE 4.2: Inductance of the in series connected two coils changes as a function of their relative axis angle

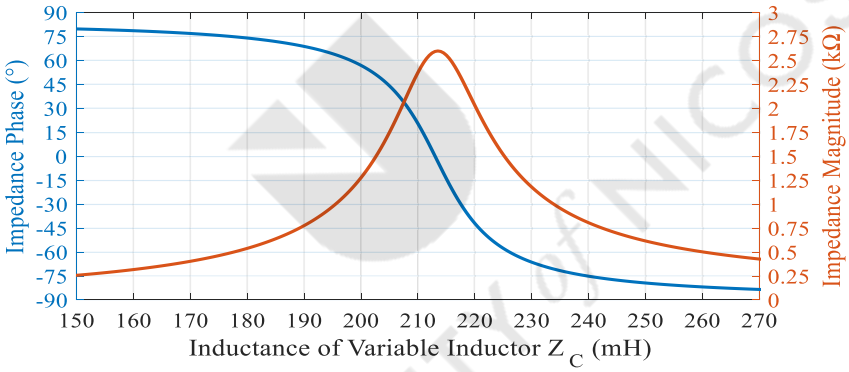

FIGURE 4.3: Inductance range with appropriate phase and magnitude plots (determined by Equation 4.1)

The analysis of power provides conclusive information with respect to active and reactive power provision by the circuit. Figure 4.4 shows that the circuit operated at 230 V, can provide maximum 100 VAR inductive reactive power and 32W losses when the variable inductor is tuned to 150 mH. When regulating the variable inductor to its maximum inductance 270 mH, the circuit provides 150 VAR capacitive reactive power with negligible losses. The active power function in Figure 4.4 documents the losses arising from the resistance of the inductors.

It is noted that the variable inductor of a bigger range of inductance can realize a higher capacitive/inductive reactive power output in the circuit. A wider range of inductance could be achieved primarily by employing bigger individual inductances of the two coils for the variable inductors as well as

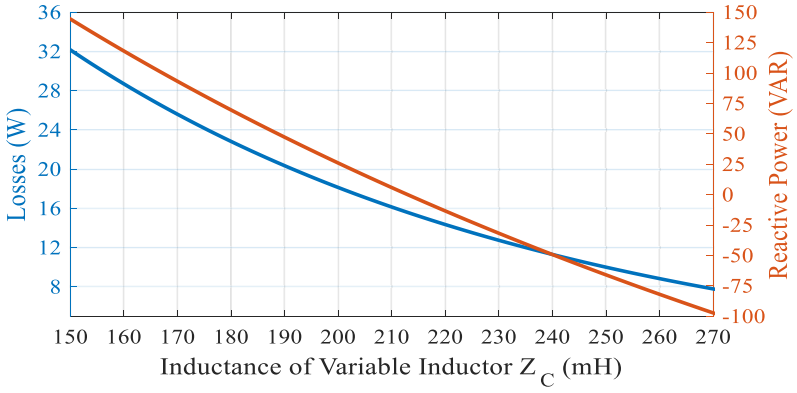

FIGURE 4.4: Inductance range with appropriate reactive power and losses

choosing the smaller coil rotating inside the bigger coil with an as big as possible diameter in order to achieve maximum flux linkage. Replacing the variable inductor by a short connection ($Z_C \rightarrow 0$) at the load terminal nodes 2 and 4 will result to a maximum possible inductive reactive power output of the circuit, in this case 850 VAR. Disconnecting, however, completely the variable inductor from nodes 2 and 4 leaving the latter as open circuit ($Z_C \rightarrow \infty$), will yield to a maximum capacitive reactive power of 750 VAR.

4.4 Experimental Part

The preceding analysis and calculations of the electric circuit are being subjected to relevant experimentation intending to document the suitability of the circuit to provide VAR compensation. The appropriate experimental setup is show in Figure 4.5. The provision of automatic capacitive reactive power compensation is demonstrated on a universal motor. The circuit destined to provide reactive power consists of 2×2 capacitors each 10 μF and two 80 mH inductors along with the variable inductor described earlier, all air wound for a linear voltage current response. A processor guided circuit regulates the automatic compensation process.

The reactive power for the two fixed operational modes mentioned earlier, has been determined via voltage, current and phase measurement of the proposed circuit subjected here to the domestic 230 V supply. Therefore, for the case that nodes 2 and 4 are shorted ($Z_C \rightarrow 0$), the impedance of the circuit becomes $Z_{13} = (19 + j58.5)\ \Omega$ with the circuit providing 815 VAR inductive reactive power and 265 W losses, whereas, when nodes 2 and 4 are left unconnected ($Z_C \rightarrow \infty$) the circuit in this condition with an impedance

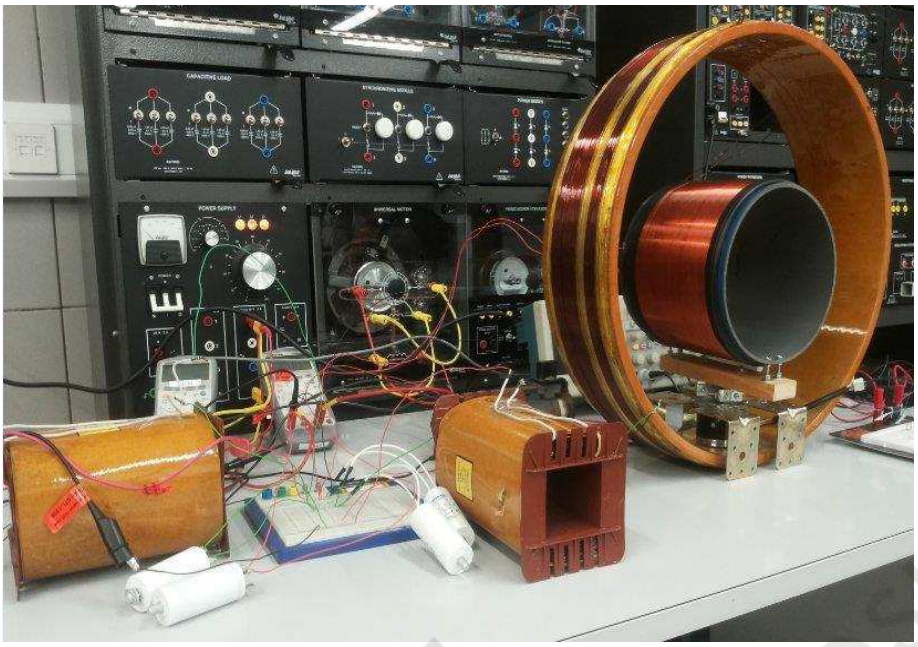

FIGURE 4.5: Electrical circuit consisting of two inductors and four capacitors appearing above to compensate the inductive reactive power of the connected universal motor in a simulated power system

$Z_{13} = (8 - j77.2)\Omega$ provides 680 VAR capacitive reactive power with 70 W losses. Inductors wound with thicker wires will result in less ohmic losses. The circuit's voltage and current presented on the oscilloscope in Figure 4.6 and Figure 4.7 show the clear inductive and capacitive character for the two fixed operational modes.

In order to provide continuous controlled reactive power under changing grid conditions, the proposed circuit has to undergo an automatic impedance adjustment. Ongoing phase determination evaluated by a microprocessor is necessary for the proposed circuit in order to adjust its reactive power provision for undergoing grid changes. The microprocessor in particular will guide the turning of the stepper motor the latter tuning the required inductance of the variable inductor to regulate the circuits terminal impedance. A 175 W universal motor operating with a P.F = 0.9 consuming 85 VAR inductive reactive power is employed in a simulated elementary single phase power system to show the concept of automatic compensation. The resulting appropriate phase in the simulated elementary power system is 26° as shown on the oscilloscope Figure 4.8.

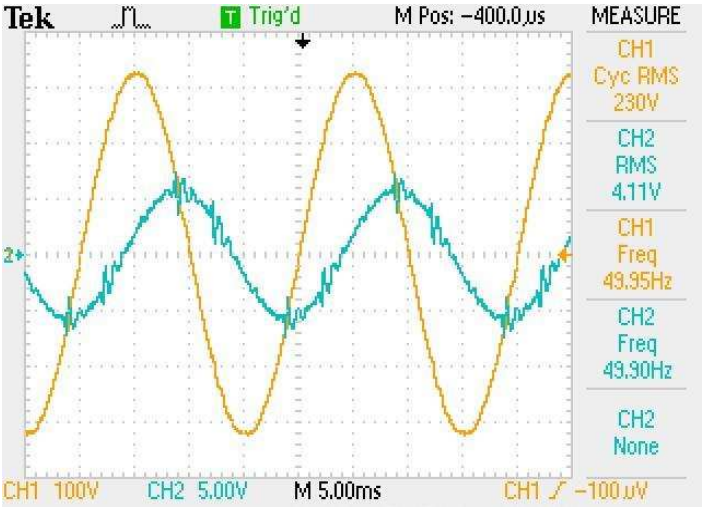

FIGURE 4.6: For shorted load terminals circuit behaves inductive as shown by the appropriate source voltage and current (the latter in blue lagging the voltage in yellow)

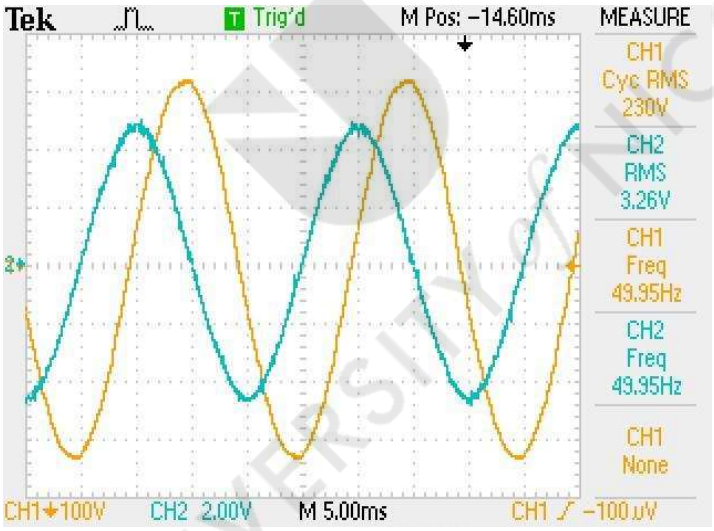

FIGURE 4.7: For open load terminals circuit behaves capacitive as shown by the appropriate source voltage and current (the latter in blue leading the voltage in yellow)

Observing the reactive power characteristic in Figure 4.4, the stepper motor will rotate until 85 VAR capacitive reactive power is being provided by the circuit. This will occur when the variable inductor has been tuned to an inductance of 265 mH. The reactive power of the motor now compensated by the proposed circuit will eliminate a phase to a 0° as shown in Figure 4.9.

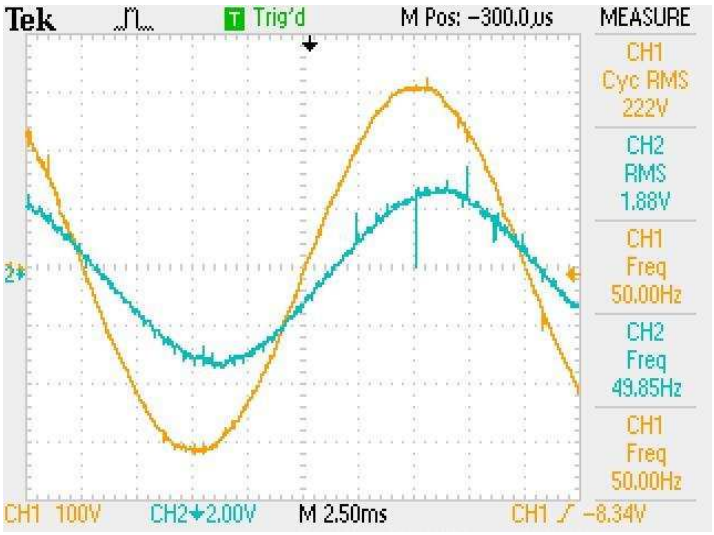

FIGURE 4.8: Moderate phase of universal motor 26°

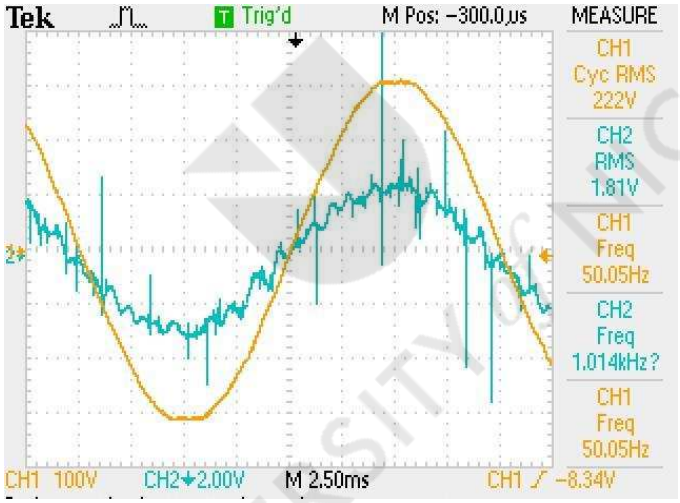

FIGURE 4.9: Reactive power of motor is compensated by regulated circuit resulting to zero phase in the simulated power system

4.5 Discussion

This chapter presented an electric circuit as an equivalent of a wound aluminum and polyester reel arranged for the conventional construction of AC power capacitors. A specific way of operating the wound aluminum and polyester foils realizes both capacitance and inductance at its terminals. Consequently significance of this circuit is the possibility to regulate its terminal

impedance within its dual character, that is, capacitive and inductive, automatically via a variable inductor connected to the circuit. The variable inductor, in turn, is tuned mechanically by a a stepper motor. The circuit, with its ability to provide both capacitive and inductive reactive power, is destined to function as a VAR compensator. To assess the later, the power characteristic as a function of variable inductor reveals the suitability of the circuit. The circuit's impedance supports preceding power analysis. The acquired knowledge about the electric circuit as an equivalent of wound foils (aluminum and polyester) will be applied on the actual foil wound integrated inductor-capacitor in the next chapter.

Chapter 5

Testing of Integrated Component as VAR Compensator

This chapter extends the integrated inductor-capacitor introduced in chapter 2 towards its control. Furthermore, the variable inductor presented and tested on its equivalent circuit in chapter 4 is presented here with the integrated inductor-capacitor control as a VAR Compensator with its power characteristics. The proposed device is tested on a 1.2 kW, 230 V motor running at a P.F of 0.75.

5.1 Concept

Previous studies in chapter 3 lead to the derivation of the equivalent circuit of wound foils shown below in Figure 5.1 without an impedance between the load terminals 2 and 4.

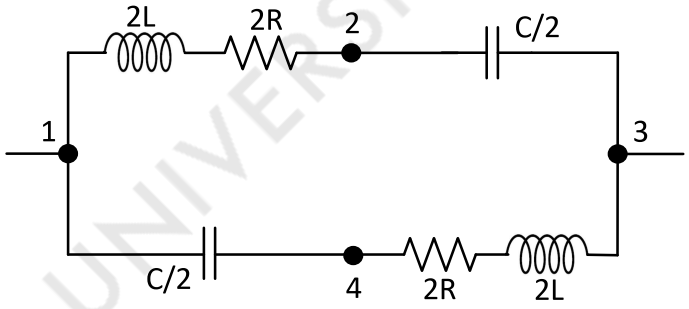

FIGURE 5.1: Wound foil's electrical equivalent circuit

The parameters of the equivalent circuit are being derived by measurements directly on the constructed pilot model in chapter 2, Figure 2.10 as described above in chapter 3. Operating the pilot model via the supply terminals 1-3 while leaving the load terminals 2-4 unconnected as one of the two fixed operational modes and ignoring the foils resistance because of its

insignificant low value as shown below in Figure 5.2 will yield the terminal impedance in Equation 5.1.

$$Z_{open} = j\left(\omega L - \frac{1}{\omega C}\right) \tag{5.1}$$

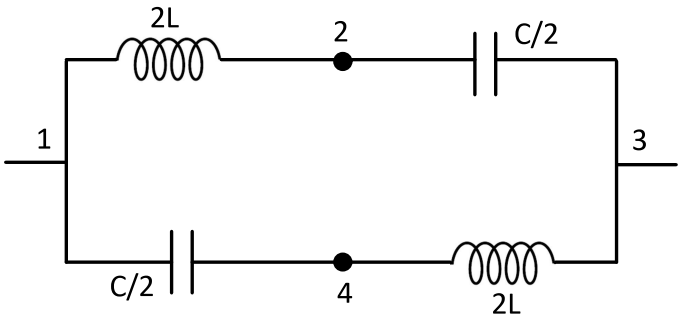

FIGURE 5.2: Equivalent circuit representation of wound foils considering control terminals/load terminals open

Shorting the load terminals 2-4 as the second fixed operational mode will yield according to the changed circuit in Figure 5.3 a terminal impedance as given by in Equation 5.2.

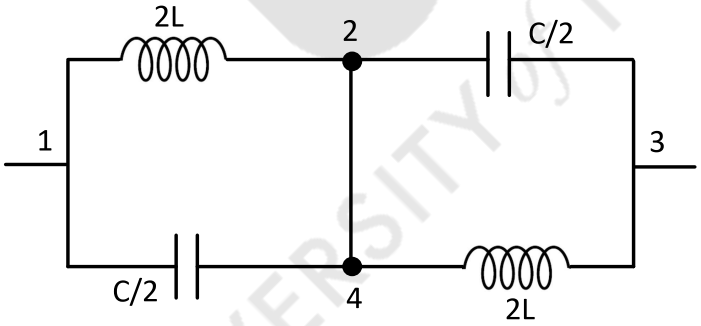

FIGURE 5.3: Equivalent circuit representation of wound foils considering control terminals/load terminals shorted

$$Z_{short} = \frac{4}{j\left(\omega C - \frac{1}{\omega L}\right)} \tag{5.2}$$

The transition between the two fixed operational modes in Figure 5.2 and Figure 5.3 can be realized by controlling the current flow between the load terminals 2-4. This can be achieved via power electronics which, however, would give rise to harmonics or by a variable impedance connected between the load terminals 2 and 4 as shown in Figure 5.4. For the present application, a variable inductor is chosen to control the terminal impedance 1-3 of

the pilot model. Such a variable inductor used in previous experiments in chapter 4 if air wound and with high quality factor does not generate harmonics and keeps losses low.

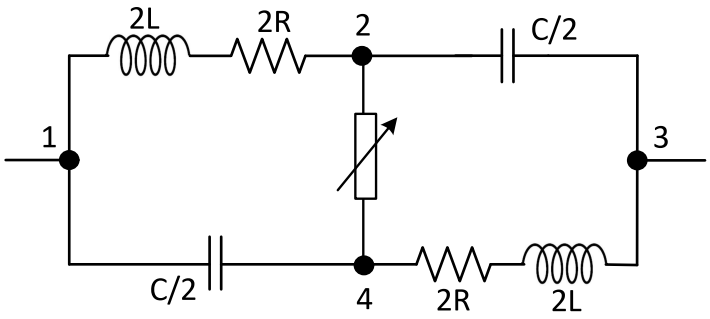

FIGURE 5.4: Termninal impedance of wound foils between 1-3 is altered via a variable impedance between 2-4

The impedance of the wound foils' equivalent (Michaelides and Nicolaou, 2017a) in Equation 5.3 is expressed as a function of the foils' inductance, capacitance, resistance, the frequency and the variable impedance Z_C.

$$Z_{13} = \frac{4j\omega L + 4R + j\omega RC \cdot Z_c + Z_c\left(1 - \omega^2 LC\right)}{j\omega C\left(R + Z_c\right) + 1 - \omega^2 LC} \tag{5.3}$$

A variable inductor in the range of 0 to 10 H may alter the terminal impedance of the component between the two fixed operational modes shown in Figure 5.2 and Figure 5.3, that is, to simulate a short or an infinite impedance. Realistic range of the variable inductor, however, permits far less impedance regulation.

The variable inductor constructed on this occasion functions on the mutual inductance principle (Satyamsetti et al., 2022) and consists of two separate cylindrical inductors connected in-series. They are adjusted such that the smaller inductor is positioned exactly in the middle of the bigger inductor and can rotate 180° on its vertical diametric axis. The small inductor has a diameter of 20 cm and an inductance of 19 mH whereas the big inductor has 50 cm diameter with an inductance of 16 mH. When initially aligned co-axially so that their magnetic fluxes oppose each other the resultant inductance is 21 mH. On rotating the small inductor via a stepper motor by 180° while the big inductor is kept stable so that their coaxial alignment is again restored, their magnetic fields reinforce resulting to an inductance of 51 mH.

The pilot model's reactive power for a varying inductance between 20-50 mH is shown on the graph of Figure 5.5 the dual character of the component

as the reactive power turns from inductive to capacitive. The graph has been calculated with Equation 5.3 for 230 V.

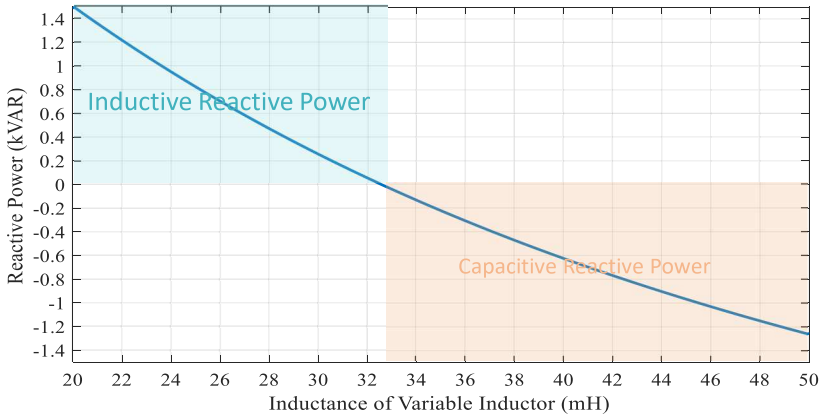

FIGURE 5.5: Calculated reactive power of integrated inductor-capacitor regulated by the variable inductor

For low values of the variable inductor the component has a lagging phase exhibiting inductive behavior. As the value of the variable inductor increases the reactive power eventually becomes capacitive. Reactive power is neither injected nor absorbed when the inductance of the variable inductor is 33 mH. In this state, the component exhibits no reactive power in the system.

It has been shown in preceding measurements that the component can compensate reactive power both inductive and capacitive to achieve a desired phase. Considering the eventual operation of this integrated component in the grid with constant shifting phase an automatic adjustment of the component would counter these changes. This can be realized by adjusting the variable inductor in the load loop between terminals 2 and 4. To achieve an immediate response of the component to changes in the grid, a monitoring unit collects continuously grid parameters and forwards them to a control unit. A processor, in turn, will regulates via the stepper motor the value of the variable inductor. Consequently, the component's terminal impedance changes to provide the required reactive power. As soon as conditions in the grid change because of an added or disconnected load, the monitoring unit sends the new values to the processor and a renewed adjustment of the variable inductor via the stepper motor alters the terminal impedance of the component to restore desired conditions.

5.2 Experimentation with Pilot Model

The final part of the study intends to demonstrate the suitability of the integrated component as a VAR compensator. For this experimental part the pilot model constructed earlier (appearing in chapter 2, Figure 2.10) is being used. The phase of a micro-scaled simulated power system caused by a motor shall be compensated by the integrated component. A 1.2 kW, 230 V motor running at a power factor of 0.75 is consuming 1.1 k VAR inductive reactive power. The load is connected in parallel to the integrated component/pilot model. The appropriate experimental arrangement and analytic electronic circuit is shown in Figure 5.6, Figure 5.9 and Figure 5.7.

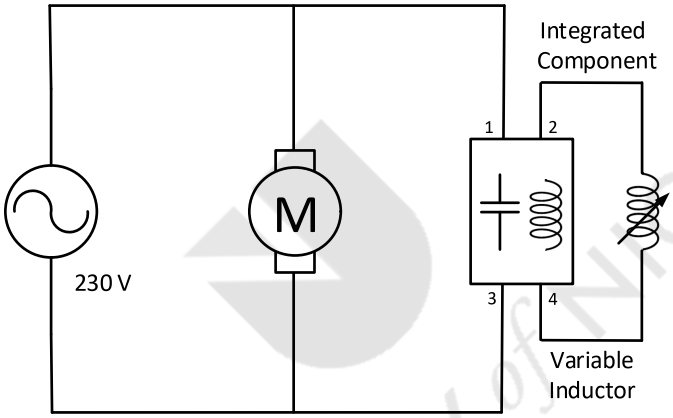

FIGURE 5.6: Experimental circuit. Variable inductor regulates terminal impedance of integrated component to provide necessary reactive power

Considering the operation of this integrated component in the grid with constantly changing phase shift, an automatic regulation of the component realized via the variable inductor can compensate changes. To achieve an immediate response of the component to changes in the grid, a monitoring unit collects continuously grid parameters and forwards them to a control unit. A processor, in turn, will regulate the variable inductor. This way, the component shall provide the required reactive power to compensate an excess grid reactive power. As soon as conditions in the grid change because of an added or withdrawn load the monitoring unit will send the new values to the processor and a renewed adjustment (that is a change of the device's terminal impedance) will take place through the variable inductor in order to retain unity power factor. A reliable assessment about dynamic compensation by

the integrated component has been possible, following experimentation with the integrated component.

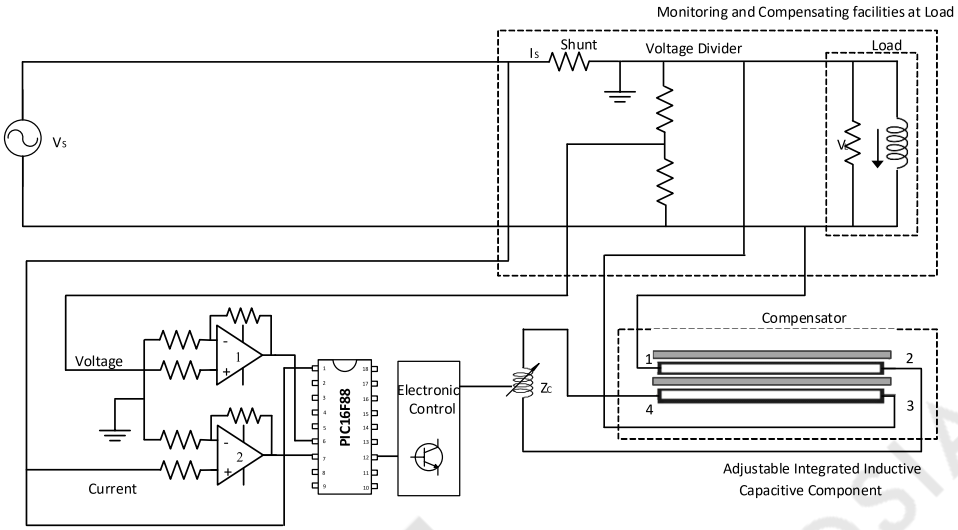

FIGURE 5.7: Analytic electronic circuit to perform automatic compensation

The pilot model shown in chapter 2, Figure 2.10 provides variable reactive power in an electronic circuit simulating the power system. The analytic electronic circuit in Figure 5.7 will provide the basic layout for the laboratory setup to experiment on dynamic compensation. It has to perform two main tasks, the continuous phase measurement and the consequent regulation of the variable inductor between the load terminals 2-4 to adjust the terminal impedance of the component. Evaluation of the load voltage is being achieved via a voltage divider and the operational amplifier 1 transforms the sinusoidal load voltage V_S to a TTL signal (5V/0V)so that the later can be forwarded as a digital signal to the processor. The analog signal across the load is initially reduced by the voltage divider to 3V in order to be entered to an operational amplifier supplied by 5 V. The analog signal is further amplified by hundred times so that the output of the operational amplifier is saturated to the form of a rectangular 5 V signal, the positive of which is in phase with the positive half of the sinusoidal input signal and the negative – 5 V of the output is in phase with the negative half of the sinusoidal input. Evaluation of the current I_S is being achieved likewise via a shunt, the voltage across which is forwarded to operational amplifier 2 and converted to a rectangular signal.

However, when the two signals enter the processor the negative part is being discarded by the processor so that the signals can be assessed by the later as typical TTL signals (5V/0V). Figure 5.8 shows the two initial sinusoidal signals, signal 1 the load voltage and signal 3 the current, converted to the respective digital signals 2 and 4.

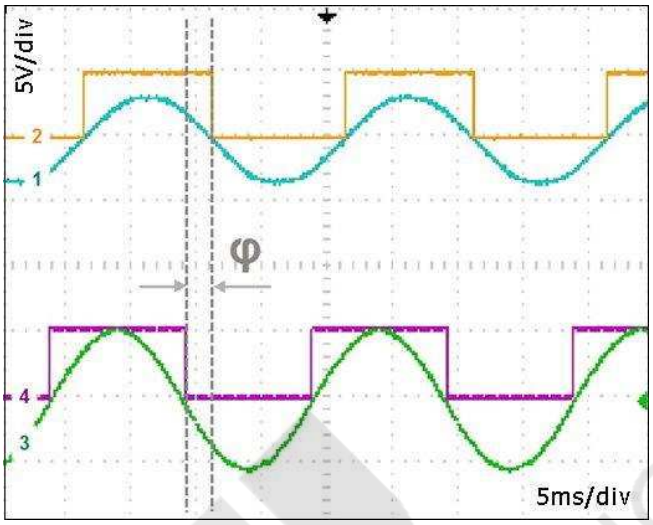

FIGURE 5.8: Source voltage and load current and their respective TTL signals

The processor calculates the phase ϕ between the two digital signals in Figure 5.8, that is, between voltage and current, via their time shift appearing on the oscilloscope on this occasion with approximately 2 ms. The processor will then further adjust the variable inductor via the stepper motor depending on the measured phase ϕ and regulate in this way the component's terminal impedance so as to provide the necessary reactive power for phase compensation.

Initially, the component is set to its neutral state (neither providing nor absorbing reactive power) by adjusting the variable inductor to 33 mH. Hence, the phase of the circuit is determined only by the inductive load appearing on the oscilloscope in Figure 5.10 with a phase of 41.4°.

According to the graph in Figure 5.5 the component can provide a capacitive reactive power of about 1.1 kVAR at 47 mH. Hence the adjusting process to compensate the reactive power of the motor is being realized by tuning the variable inductor with the stepper motor via phase assessment of the processor in a feedback loop to the value of 47 mH. The analytic electronic circuit to perform automatic phase regulation is presented in (Satyamsetti, 2021).

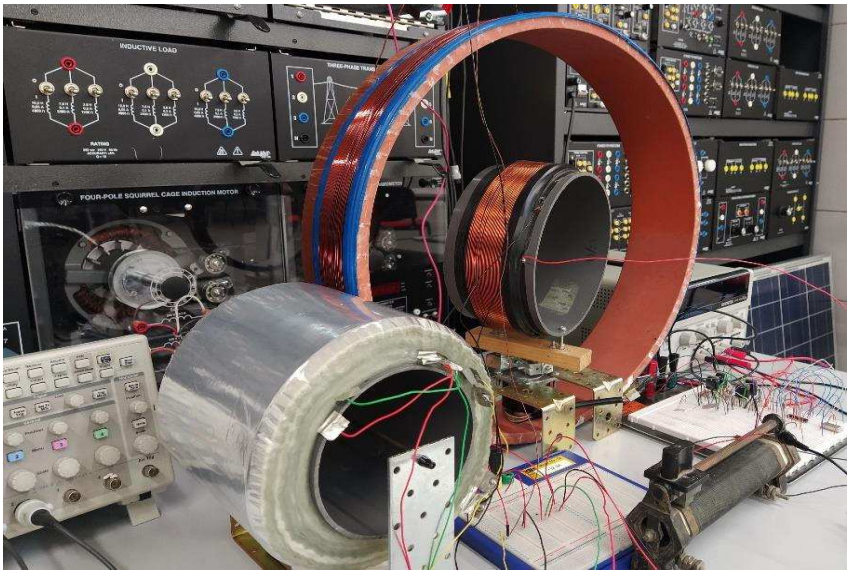

FIGURE 5.9: Integrated component featuring in the front connected to the variable inductor

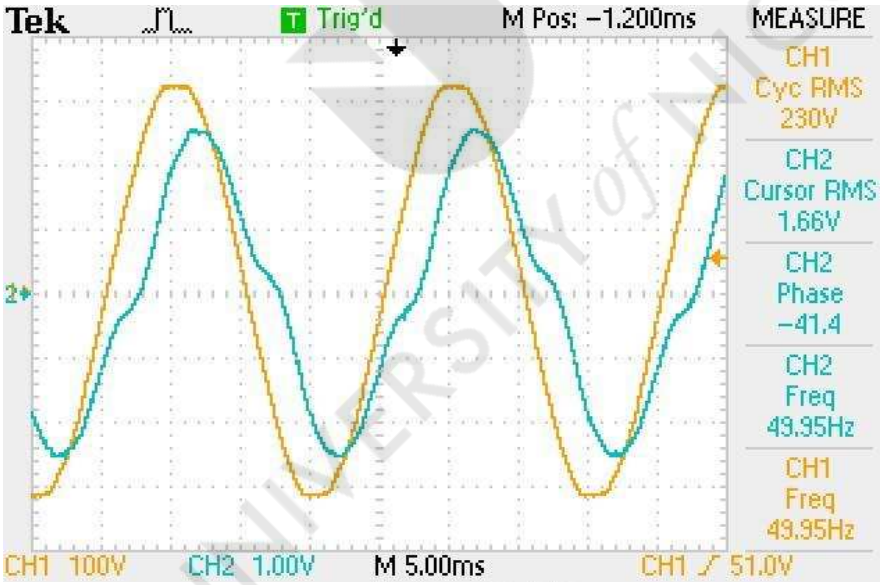

FIGURE 5.10: Phase of micro-scaled power system caused by motor while integrated component/pilot model is idle

In this state the phase of the micro scaled power system is zero as shown in Figure 5.11 and the compensation process is completed.

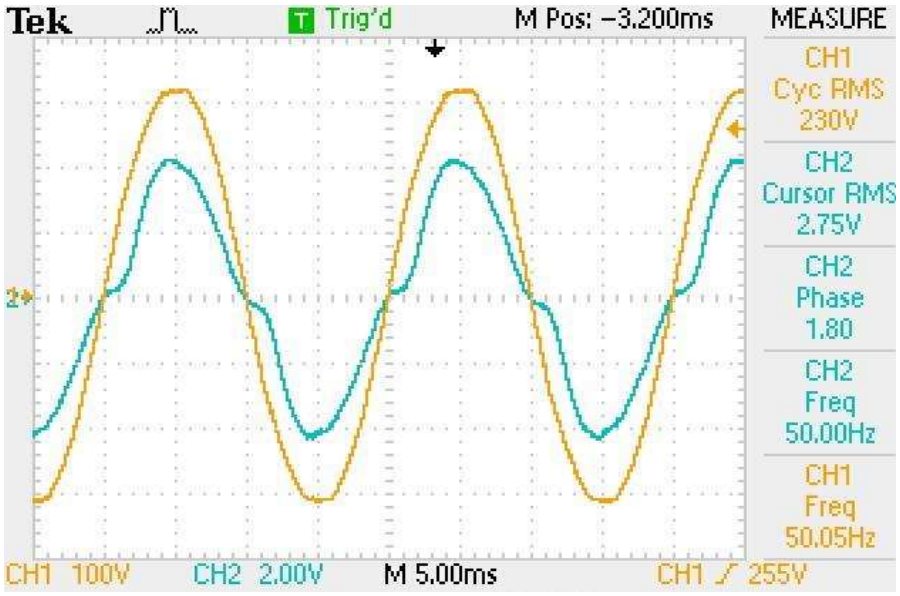

FIGURE 5.11: Reactive power of motor is compensated reflected by zero phase shift

5.3 Discussion

This chapter demonstrated clearly the concept of the constructed variable integrated inductor-capacitor with respect to its applicability as a VAR compensator by providing capacitive reactive power for the compensation of an induction motor during quantitative experimentation. Automatic compensation has been realized by a qualified electronic design via a monitoring/control/feedback algorithm.

Chapter 6

Conclusion

The preceding work presents the foil wound capacitor in its basic structure extending its operation via a specific connection of the foils to an integrated inductive-capacitive component. The concept lies in the formation of the inductance resulting from the wound aluminum foils. The significance of the foils' arrangement is their division in many small segments wound simultaneously on the same core, all connected in parallel. Thus a quality factor of the component's inductance comparable to that of discrete component wire wound inductors may be achieved.

A consequent objective of the wound foils' analysis operating in the integrated mode is the derivation of an electrical equivalent. Extensive measurements conducted on the four ends of the two aluminum foils led to a four-pole equivalent, a circuit with four terminals consisting of discrete components enabling thus its construction and hence the simulation of the integrated component's behavior for different operational scenarios with no need to wind repeatedly new foil arrangements for specific measurements. The significance of this four terminal component is its dual character capable of realizing both inductive and capacitive terminal impedance on one hand and a gradual uniform transition between these two reactive states on the other hand. Calculations on the equivalent circuit constructed with discrete components and experimentation with the latter showed that its impedance can be regulated by means of a variable resistor connected at the load terminals. However, considerable losses resulting on the variable resistor when regulating the equivalent's impedance led to a reassessment of the regulation using an air wound inductor instead. The variable inductor constructed for this purpose functions on the mutual inductance principle and consists of two separate in series connected cylindrical inductors. They are adjusted such that the smaller inductor is positioned exactly in the middle of the bigger inductor and can rotate 180° on its vertical diametric axis. The inside inductor is mounted on a stepper motor and can be turned such that the

magnetic fields of the two inductors reinforce or oppose each other yielding between maximum and minimum inductance, respectively.

Eventual application of the integrated component capable to acquire a capacitive as well as inductive terminal impedance foresees the compensation of capacitive and inductive reactive power in the grid, respectively.

Extended experimentation realizes via qualified electronics a monitoring-control-feedback algorithm that performs automatic compensation within a certain range of capacitive and inductive reactive power. Continuous assessment of the phase in a production unit will regulate via a processor and electronics control the integrated component so as to provide the required reactive power. When the reactive load changes either by connecting or disconnecting additional motors, the processor shall reassess the phase and initiate renewed an increase or decrease of the component's power in successive small steps until the phase of the system is restored to the desired value. Hence the necessity to compensate on-site inductive reactive power of motors in a small factory can be dealt with such integrated components. As of this the employment of such an integrated component is considered to be especially advantageous for plants in which the phase may change frequently within lagging and leading. For the case that the load is purely resistive, the integrated component is tuned neutral, that is, its terminal reactance is zero. The present low power experimental circuit demonstrates the concept of automatic compensation. Further experimentation on automatic compensation is expected to move towards circuits of higher power ratings testing the ability of such integrated components to switch among reactive power extremities. Considering such an integrated component with industrial parameters will have to engage in a qualified heat balance analysis to ensure the dissipation of heat created in the aluminum foils. The current state of development suggests reasonable prospects to employ such an integrated component in the power system for reactive power compensation.

Appendix A

Alternative Way to Solve Electrical Equivalent Circuit

Considering Figure 3.3 to solve for Z_{13} by applying Mesh-Analysis

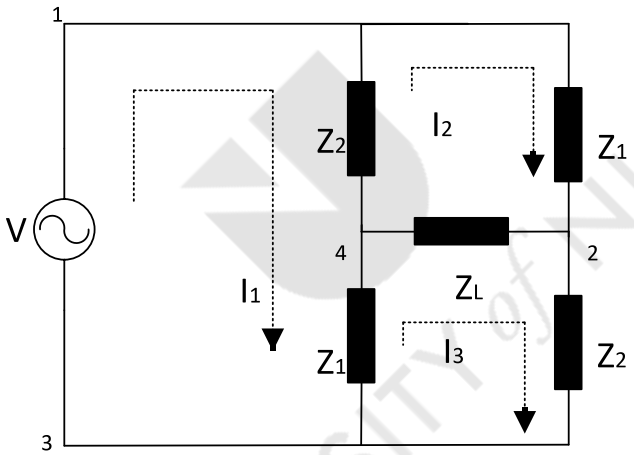

FIGURE A.1: Applying mesh-analysis to the equivalent circuit

$$I_1 (Z_1 + Z_2) - Z_2 I_2 - Z_3 I_3 = V \tag{A.1}$$

$$I_2 (Z_1 + Z_2 + Z_3) - Z_2 I_1 - Z_3 I_3 = 0 \tag{A.2}$$

$$I_3 (Z_1 + Z_2 + Z_3) - Z_1 I_1 - Z_3 I_2 = 0 \tag{A.3}$$

$$I_1 (Z_1 + Z_2) - Z_2 I_2 - Z_3 I_3 = V \tag{A.4}$$

$$I_1 (-Z_2) + (Z_1 + Z_2 + Z_3) I_2 - Z_3 I_3 = 0 \tag{A.5}$$

$$I_1 (-Z_1) - Z_3 I_2 + (Z_1 + Z_2 + Z_3) I_3 = 0 \tag{A.6}$$

$$I_1 = \frac{\left|\begin{pmatrix} V & -Z_2 & -Z_1 \\ 0 & Z_1+Z_2+Z_3 & -Z_3 \\ 0 & -Z_3 & Z_1+Z_2+Z_3 \end{pmatrix}\right|}{\left|\begin{pmatrix} Z_1+Z_2 & -Z_2 & -Z_1 \\ -Z_2 & Z_1+Z_2+Z_3 & -Z_3 \\ -Z_1 & -Z_3 & Z_1+Z_2+Z_3 \end{pmatrix}\right|} \tag{A.7}$$

$$I_1 = \frac{V(Z_1+Z_2+Z_3)^2 - VZ_3^2}{(Z_1+Z_2+Z_3)^2(Z_1+Z_2) - 2Z_1Z_2Z_3 - Z_1^2(Z_1+Z_2+Z_3) - Z_3^2(Z_1+Z_2) - Z_2^2(Z_1+Z_2+Z_3)} \tag{A.8}$$

$$Z_{13} = \frac{(Z_1+Z_2+Z_3)^2(Z_1+Z_2) - 2Z_1Z_2Z_3 - Z_1^2(Z_1+Z_2+Z_3) - Z_3^2(Z_1+Z_2) - Z_2^2(Z_1+Z_2+Z_3)}{(Z_1+Z_2+Z_3)^2 - Z_3^2} \tag{A.9}$$

$$Z_{13} = \frac{(Z_1+Z_2+Z_3)\left[(Z_1+Z_2)(Z_1+Z_2+Z_3) - Z_1^2 - Z_2^2\right] - 2Z_1Z_2Z_3 - Z_3^2(Z_1+Z_2)}{(Z_1+Z_2+Z_3-Z_3)(Z_1+Z_2+Z_3+Z_3)} \tag{A.10}$$

$$Z_{13} = \frac{(Z_1+Z_2+Z_3)[2Z_1Z_2+Z_1Z_3+Z_2Z_3] - 2Z_1Z_2Z_3 - Z_3^2Z_1 - Z_3^2Z_2}{(Z_1+Z_2)(Z_1+Z_2+Z_3)} \tag{A.11}$$

$$Z_{13} = \frac{\left[2Z_1^2Z_2 + Z_1^2Z_3 + Z_1Z_2Z_3 + 2Z_1Z_2^2 + Z_1Z_2Z_3 + Z_2^2Z_3 + 2Z_1Z_2Z_3 + Z_1Z_3^2 + Z_3^2Z_2 - 2Z_1Z_2Z_3 - Z_3^2Z_1 - Z_3^2Z_2\right]}{(Z_1+Z_2)(Z_1+Z_2+Z_3)} \tag{A.12}$$

$$Z_{13} = \frac{2Z_1Z_2Z_3 + 2Z_1Z_2^2 + 2Z_1^2Z_2 + Z_3Z_1^2 + Z_3Z_1^2}{(Z_1 + Z_2)(Z_1 + Z_2 + Z_3)} \tag{A.13}$$

$$Z_{13} = \frac{2Z_1Z_2(Z_1 + Z_2) + Z_3(Z_1 + Z_2)^2}{(Z_1 + Z_2)(Z_1 + Z_2 + Z_3)} \tag{A.14}$$

$$Z_{13} = \frac{(Z_1 + Z_2)(2Z_1Z_2 + Z_1Z_3 + Z_2Z_3)}{(Z_1 + Z_2)(Z_1 + Z_2 + Z_3)} \tag{A.15}$$

Substituting $Z_1 = 2R + 2j\omega L, Z_2 = {}^{-2j}/_{\omega C}, Z_3 = R_L$ in A.15 we get A.16

$$Z_{13} = \frac{\left[(4R + 4j\omega L)\left(\frac{-2j}{\omega C}\right)\right] + \left(2R + 2j\omega L - \frac{2j}{\omega C}\right)}{2R + 2j\omega L - \frac{2j}{\omega C} + 2R_L} \tag{A.16}$$

$$Z_{13} = \frac{\left(\frac{-2j}{\omega C}\right)[(4R + 4j\omega L)] + \left(\frac{2\omega RC + 2j\omega^2 LC - 2j}{\omega C}\right)R_L}{\left(\frac{-2j}{\omega C}\right)[j\omega RC + j\omega R_L RC - \omega^2 LC + 1]} \tag{A.17}$$

$$Z_{13} = \frac{4R + 4j\omega L + j\omega RC \cdot R_L + R_L(1 - \omega^2 LC)}{j\omega C(R + R_L) + 1 - \omega^2 LC} \tag{A.18}$$

Bibliography

Chavez, Cesar and John A. Houdek (2007). "Dynamic Harmonic Mitigation and power factor correction". In: *2007 9th International Conference on Electrical Power Quality and Utilisation*, pp. 1–5. DOI: 10.1109/EPQU.2007.4424144.

Chen, Jen-Hung, Wei-Jen Lee, and Mo-Shing Chen (1999). "Using a static VAr compensator to balance a distribution system". In: *IEEE Transactions on Industry Applications* 35.2, pp. 298–304. DOI: 10.1109/28.753620.

Dixon, J. et al. (2005). "Reactive Power Compensation Technologies: State-of-the-Art Review". In: *Proceedings of the IEEE* 93.12, pp. 2144–2164. DOI: 10.1109/JPROC.2005.859937.

Fehr, Ralph (2016). "Power Factor Correction". In: *Industrial Power Distribution*, pp. 319–333. DOI: 10.1002/9781119065180.ch11.

Haque, S E, N H Malik, and W Shepherd (1985). "Operation of a Fixed Capacitor-Thyristor Controlled Reactor (FC-TCR) Power Factor Compensator". In: *IEEE Transactions on Power Apparatus and Systems* PAS-104.6, pp. 1385–1390. DOI: 10.1109/TPAS.1985.319231.

Jaramillo, S.H., G.T. Heydt, and E. O'Neill-Carrillo (2000). "Power quality indices for aperiodic voltages and currents". In: *IEEE Transactions on Power Delivery* 15.2, pp. 784–790. DOI: 10.1109/61.853020.

Jovanovic, M.M. and Y. Jang (2005). "State-of-the-art, single-phase, active power-factor-correction techniques for high-power applications - an overview". In: *IEEE Transactions on Industrial Electronics* 52.3, pp. 701–708. DOI: 10.1109/TIE.2005.843964.

Lembeye, Y., P. Goubier, and J.-P. Ferrieux (2005). "Integrated planar L-C-T component: Design,Characterization and Experimental Efficiency analysis". In: *IEEE Transactions on Power Electronics* 20.3, pp. 593–599. DOI: 10.1109/TPEL.2005.846558.

Lin, Tao and A. Domijan (2005). "On power quality indices and real time measurement". In: *IEEE Transactions on Power Delivery* 20.4, pp. 2552–2562. DOI: 10.1109/TPWRD.2005.852333.

Ma, Youjie et al. (2016). "The discussion on static synchronous compensator technology". In: *2016 IEEE International Conference on Mechatronics and Automation*, pp. 106–111. DOI: 10.1109/ICMA.2016.7558543.

Michael Casper, William Mraz (U.S. Patent 7,446,388 B29). *Integrated thin film capacitor/inductor/interconnect system and method*. URL: https://patents.google.com/patent/US20040081811.

Michaelides, Andreas (2015). "Integrated inductive-capacitive component used as a filter for harmonic modulations in the grid". In: *2015 13th International Conference on Engineering of Modern Electric Systems (EMES)*, pp. 1–4. DOI: 10.1109/EMES.2015.7158389.

Michaelides, Andreas and Thanos Nicolaou (2017a). "Electrical equivalent of wound aluminum foils". In: *2017 10th International Symposium on Advanced Topics in Electrical Engineering (ATEE)*, pp. 98–102. DOI: 10.1109/ATEE.2017.7905151.

— (2017b). "Starting and running the induction motor with a variable capacitor". In: *2017 14th International Conference on Engineering of Modern Electric Systems (EMES)*, pp. 87–90. DOI: 10.1109/EMES.2017.7980388.

— (2021). "Constructing an Integrated Inductive-Capacitive Component to Filter Harmonic Modulations". In: *IEEE Transactions on Power Delivery* 36.4, pp. 2109–2117. DOI: 10.1109/TPWRD.2020.3020703.

Miyashita, Shuhei et al. (2014). "Self-folding printable elastic electric devices: Resistor, capacitor, and inductor". In: *2014 IEEE International Conference on Robotics and Automation (ICRA)*, pp. 1446–1453. DOI: 10.1109/ICRA.2014.6907042.

Narain G. Hingorani, Laszlo Gyugyi (1999). *Understanding FACTS Concepts and Technology of Flexible AC Transmission Systems*.

Pop, O. et al. (2001). "Power factor correction circuit with a new modified SEPIC converter". In: *24th International Spring Seminar on Electronics Technology. Concurrent Engineering in Electronic Packaging. ISSE 2001. Conference Proceedings (Cat. No.01EX492)*, pp. 117–120. DOI: 10.1109/ISSE.2001.931026.

Rahmani, Salem et al. (2014). "A Combination of Shunt Hybrid Power Filter and Thyristor-Controlled Reactor for Power Quality". In: *IEEE Transactions on Industrial Electronics* 61.5, pp. 2152–2164. DOI: 10.1109/TIE.2013.2272271.

Reeves, R. (1978). "Air-cored foil-wound inductors". English. In: *Proceedings of the Institution of Electrical Engineers* 125 (5), 460–464(4). ISSN: 0020-3270.

URL: https://digital-library.theiet.org/content/journals/10.1049/piee.1978.0111.

R.Mohan Mathur, Rajiv K.Varma (2002). *Thyristor-based FACTS Controllers for Electrical Transmission Systems*.

Satyamsetti, V. K. (2021). "ACTIVE COMPENSATION OF REACTIVE POWER VIA STATCOM ANALYSIS". English. In: *IET Conference Proceedings*, 121–126(5). URL: https://digital-library.theiet.org/content/conferences/10.1049/icp.2021.1252.

Satyamsetti, Vijayakrishna et al. (2022). "A Novel Simple Inductor-Controlled VAR Compensator". In: *IEEE Transactions on Circuits and Systems II: Express Briefs* 69.2, pp. 524–528. DOI: 10.1109/TCSII.2021.3099876.

Sebastian, J. and M. Jaureguizar (1993). "Future trends in power factor correction in power systems". In: *Proceedings of the 1993 Power Electronics Congress (Congreso Internacional de Electronica de Polentia)*, pp. 136–153. DOI: 10.1109/CIEP.1993.379459.

Teleke, Sercan et al. (2008). "Dynamic Performance Comparison of Synchronous Condenser and SVC". In: *IEEE Transactions on Power Delivery* 23.3, pp. 1606–1612. DOI: 10.1109/TPWRD.2007.916109.

Thanachayanont, A. (2000). "A 1.5-V high-Q CMOS active inductor for IF/RF wireless applications". In: *IEEE APCCAS 2000. 2000 IEEE Asia-Pacific Conference on Circuits and Systems. Electronic Communication Systems. (Cat. No.00EX394)*, pp. 654–657. DOI: 10.1109/APCCAS.2000.913605.

T.J.Miller (2017). *Reactive Power Control in Electric Systems*.

Yong Hua Song, Allan T. Johns (2008). *Flexible AC Transmission System*.

Yuan, Fei (2008). *CMOS Active Inductors and Transformers. Principle, implementation, and applications*.